iScience

CellPress
OPEN ACCESS

Article

An EZH2-NF-κB regulatory axis drives expression of pro-oncogenic gene signatures in triple negative breast cancer

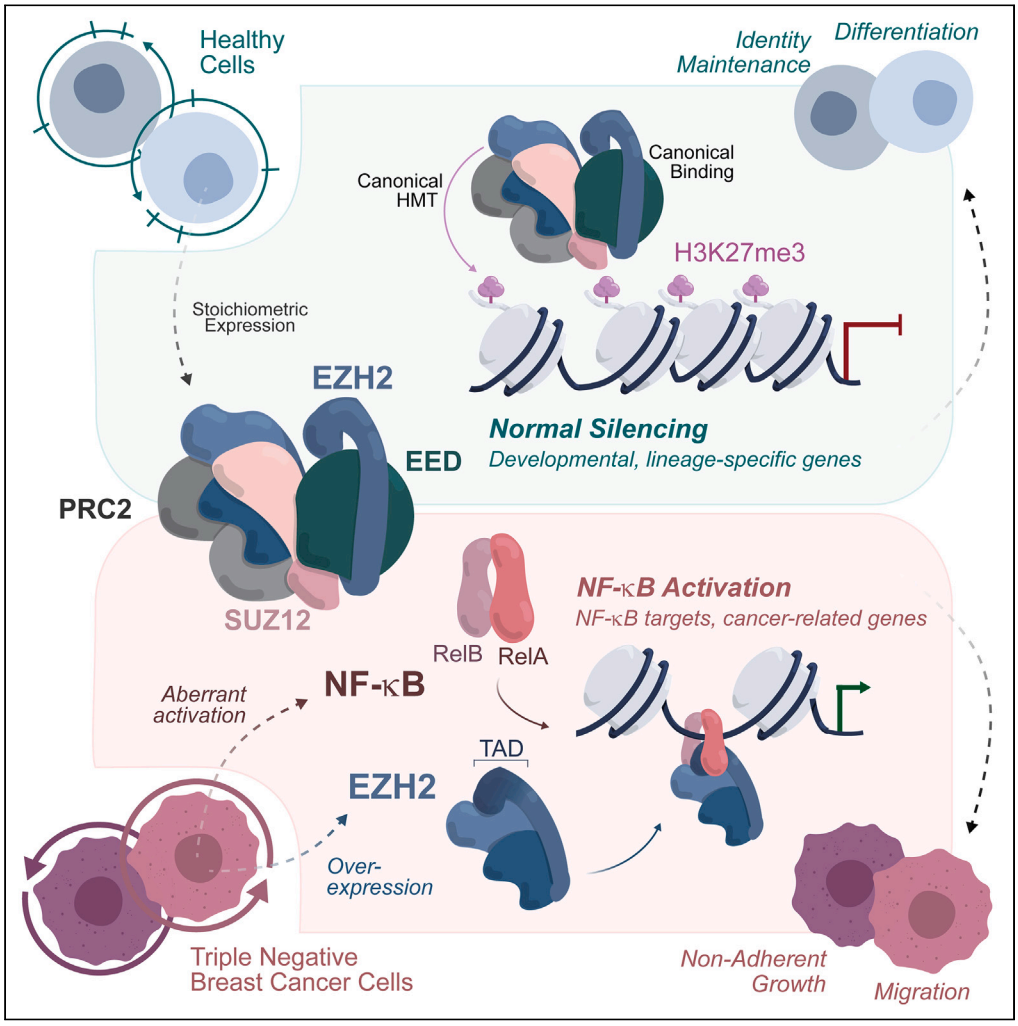

Gabrielle J. Dardis, Jun Wang, Jeremy M. Simon, Gang Greg Wang, Albert S. Baldwin

abaldwin@med.unc.edu

Highlights

EZH2 and RelA co-activate transcription of a subset of NF-κB target genes

EZH2 physically interacts with RelA via the transactivation domain

EZH2 functional interaction with NF-κB is PRC2-independent

EZH2-NF-κB activated genes are enriched in aggressive breast cancer subtypes

Dardis et al., iScience 26, 107115
July 21, 2023
https://doi.org/10.1016/j.isci.2023.107115

iScience

CellPress
OPEN ACCESS

Article

An EZH2-NF-κB regulatory axis drives expression of pro-oncogenic gene signatures in triple negative breast cancer

Gabrielle J. Dardis,[1,2] Jun Wang,[1,2] Jeremy M. Simon,[1,3,4] Gang Greg Wang,[1,2] and Albert S. Baldwin[1,5,*]

SUMMARY

The histone methyltransferase EZH2 has been studied most extensively in the context of PRC2-dependent gene repression. Accumulating evidence indicates non-canonical functions for EZH2 in cancer contexts including promoting paradoxical gene expression through interactions with transcription factors, including NF-κB in triple negative breast cancer (TNBC). We profile EZH2 and NF-κB factor co-localization and positive gene regulation genome-wide, and define a subset of NF-κB targets and genes associated with oncogenic functions in TNBC that is enriched in patient datasets. We demonstrate interaction between EZH2 and RelA requiring the recently identified transactivation domain (TAD) which mediates EZH2 recruitment to, and activation of certain NF-κB-dependent genes, and supports downstream migration and stemness phenotypes in TNBC cells. Interestingly, EZH2-NF-κB positive regulation of genes and stemness does not require PRC2. This study provides new insight into pro-oncogenic regulatory functions for EZH2 in breast cancer through PRC2-independent, and NF-κB-dependent regulatory mechanisms.

INTRODUCTION

Enhancer of zeste homology 2 (EZH2) is the catalytic histone methyltransferase (HMT) subunit of polycomb repressive complex 2 (PRC2). EZH2 and additional PRC2 subunits, including core subunits SUZ12 and EED, function together to catalyze the trimethylation of lysine 27 on histone H3 (H3K27me3), which contributes to gene silencing and heterochromatin formation.[1–4] This activity is critical for embryonic development and cell-specific gene expression, including silencing of specific genes in order to facilitate lineage commitment, and EZH2 expression typically decreases as cells terminally differentiate.[5,6] However, in addition to mutation and deregulation, EZH2 is overexpressed in multiple types of hematological and solid tumors, and this has been strongly associated with aggressive tumor subtypes and oncogenic activity including high proliferation rate, tumor suppressor gene silencing, cancer progression, and poor patient outcomes.[7–14] Thus, targeting EZH2 is of considerable clinical interest.[15,16] The current therapeutic strategy largely focuses on traditional small molecule inhibitors to target the canonical catalytic activity of EZH2, with additional approaches to disrupt or degrade PRC2 complex components.[17–22] However, HMT inhibitors may exert only partial responses and other "epidrugs" when used as a monotherapy may face primary resistance in solid tumors, including those where EZH2 may be overexpressed and dysregulated.[23–26] Another barrier to therapeutic efficacy is reported non-canonical activity of EZH2 that may contribute to disease independently of HMT activity or PRC2 protein interactions, and which current approaches would fail to target.[27–31]

Non-canonical functions of EZH2 vary and appear context-dependent, but have included methylation of non-histone substrates and non-PRC2 interactions with transcription factors to promote gene expression.[27] For example, EZH2 has been shown to interact with the androgen receptor (AR) to promote gene expression in castration-resistant prostate cancer (CRPC), and to methylate STAT3 to promote downstream signaling in glioblastoma.[29,32,33] Combinations of these activities with canonical functions have also been reported that underscore the spectrum on which non-canonical EZH2 can be characterized. For instance, in Xu et al., it was shown that EZH2 functions independently of PRC2 in CRPC cells, yet requires an intact methyltransferase domain.[28]

[1]Lineberger Comprehensive Cancer Center, University of North Carolina at Chapel Hill School of Medicine, Chapel Hill, NC 27599, USA

[2]Department of Biochemistry and Biophysics, University of North Carolina at Chapel Hill School of Medicine, Chapel Hill, NC 27599, USA

[3]Department of Genetics, University of North Carolina at Chapel Hill School of Medicine, Chapel Hill, NC 27599, USA

[4]UNC Neuroscience Center, University of North Carolina at Chapel Hill, Chapel Hill, NC 27599, USA

[5]Lead contact

*Correspondence: abaldwin@med.unc.edu

https://doi.org/10.1016/j.isci.2023.107115

In triple negative breast cancer (TNBC) and closely related basal-like breast cancer (BLBC) subtypes, EZH2 is overexpressed and in these contexts has been implicated in tumorigenesis and metastasis and characterized as an oncogene.[8,34–39] TNBC/BLBC tumors are generally more aggressive and often present a worse prognosis for patients than other breast cancer subtypes, and further exhibit constitutively active inflammatory signaling via NF-κB which is additionally implicated in malignancy.[40–48] Interestingly, EZH2 was reported to interact with NF-κB transcription factors RelA and RelB to activate genes including *IL6* in TNBC cells.[30] Additionally, our group showed in TNBC cells that EZH2, in an HMT-independent manner, drives transcription of *RELB* which, in addition to being an NF-κB transcription factor and target gene, is also individually implicated in hormone-negative breast cancers.[49–51] However, the mechanism by which EZH2 activated NF-κB transcription was unexplored in these reports. A partially disordered transactivation domain (TAD) was recently identified in EZH2 that suggests a mechanism reconciling the paradoxical ability of EZH2 to promote gene expression with canonical repressive activity.[52] We (J.W. and G.G.W.) recently showed that the EZH2 TAD interacted with cMyc and p300 in mixed lineage-rearranged (MLL-r) leukemia to mediate gene activation, and EZH2 TAD interactions with AR and its splice variant in CRPC were demonstrated to promote oncogenic phenotypes and tumorous transformation.[31,53]

Here, we present evidence supporting non-canonical EZH2 activation of NF-κB in TNBC that expands upon previous reports, especially considering NF-κB signaling and TNBC context. We integrate genome-wide DNA localization of EZH2 with transcriptomic profiling to describe the landscape of non-canonical EZH2 activation in TNBC cell lines. We couple this with analysis of RelA, RelB, and NFKB2 to identify a subset of co-occupied and co-activated NF-κB target genes, including genes such as *CYR61/CCN1* that are known to promote the TNBC oncogenic phenotype.[54–56] This transcriptional co-activation, as well as contribution to migration and tumorsphere phenotypes appears dependent on physical interaction between EZH2 TAD and RelA, and we further show EZH2 functional interaction with NF-κB is PRC2-independent. Biologically, blocking EZH2 but not PRC2 components suppresses NF-κB target gene activation and tumorsphere formation. Importantly, this identified EZH2-NF-κB regulated gene set was shown to be enriched in TNBC patient samples.

RESULTS

EZH2 colocalizes with NF-κB transcription factors at NF-κB and cancer-related target genes

In addition to canonical functions as a gene repressor, EZH2 is reported to transcriptionally activate genes in cancer contexts, including TNBC cells.[30,51] To profile EZH2 activity in TNBC cells, we first performed ChIP-sequencing of the TNBC cell lines MDA-MB-231 and SUM149. In MDA-MB-231 cells, we identified 22850 EZH2 peaks that overlapped with 6981 genes (gene body +/− 5kb) and 5655 gene promoters (transcription start site (TSS) +/− 5kb). In SUM149 cells, we identified 3068 EZH2 peaks overlapping 1163 genes and 970 gene promoters (Table S1). EZH2-bound genes ($EZH2^+$) included canonical target genes *DAB2IP* and *MYT1*, and gene set enrichment analysis (GSEA) revealed significant enrichment for developmental gene sets in both cell lines (Figures 1A and S1A).[57,58]

As a transcriptional activator, EZH2 has been described to localize to genes independently of its canonical activity. Thus, we compared EZH2 chromatin binding data in MDA-MB-231 cells to publicly available MDA-MB-231 ChIP-seq data of the repressive mark H3K27me3, active gene and enhancer marks H3K4me3 and H3K27ac, and ATAC-seq signal as a measure of chromatin accessibility (Figures 1B and GEO: GSE77772, GEO: GSE72141).[59–61] From these comparisons, we distinguished two populations of EZH2-bound sites where approximately 75% of sites were conincident with repressive H3K27me3 signal ($EZH2^+/K27me3^+$, top row; 17294/22850), and approximately 25% of sites were coincident with multiple marks of open, active chromatin ($EZH2^+/K27me3^-$, bottom row; 5556/22850), suggesting this population of EZH2 may localize to active genes.

Following our group's and others' reports of functional interaction between EZH2 and NF-κB in TNBC cells, we performed motif analysis of MDA-MB-231 EZH2 peaks and found rel-homology domain (RHD) binding motifs corresponding to NF-κB transcription factors RelA (p65) and p50/p52 among the significantly enriched results (Figure S1B, Table S2).[62–64] Further, NF-κB RHD motifs were also among significantly enriched results for $EZH2^+/H3K27me3^-$ sites (Figure S1C, Table S2). We hypothesized NF-κB transcription factors may colocalize with EZH2 as co-activators at *RELB* and other target promoters, and first performed ChIP-qPCR for EZH2 and factors RelA (which can activate *RELB*), p100/p52 (encoded by *NFKB2*, which frequently heterodimerizes with RelB) and RelB itself in MDA-MB-231 and SUM149 cells.[65–67] At both a

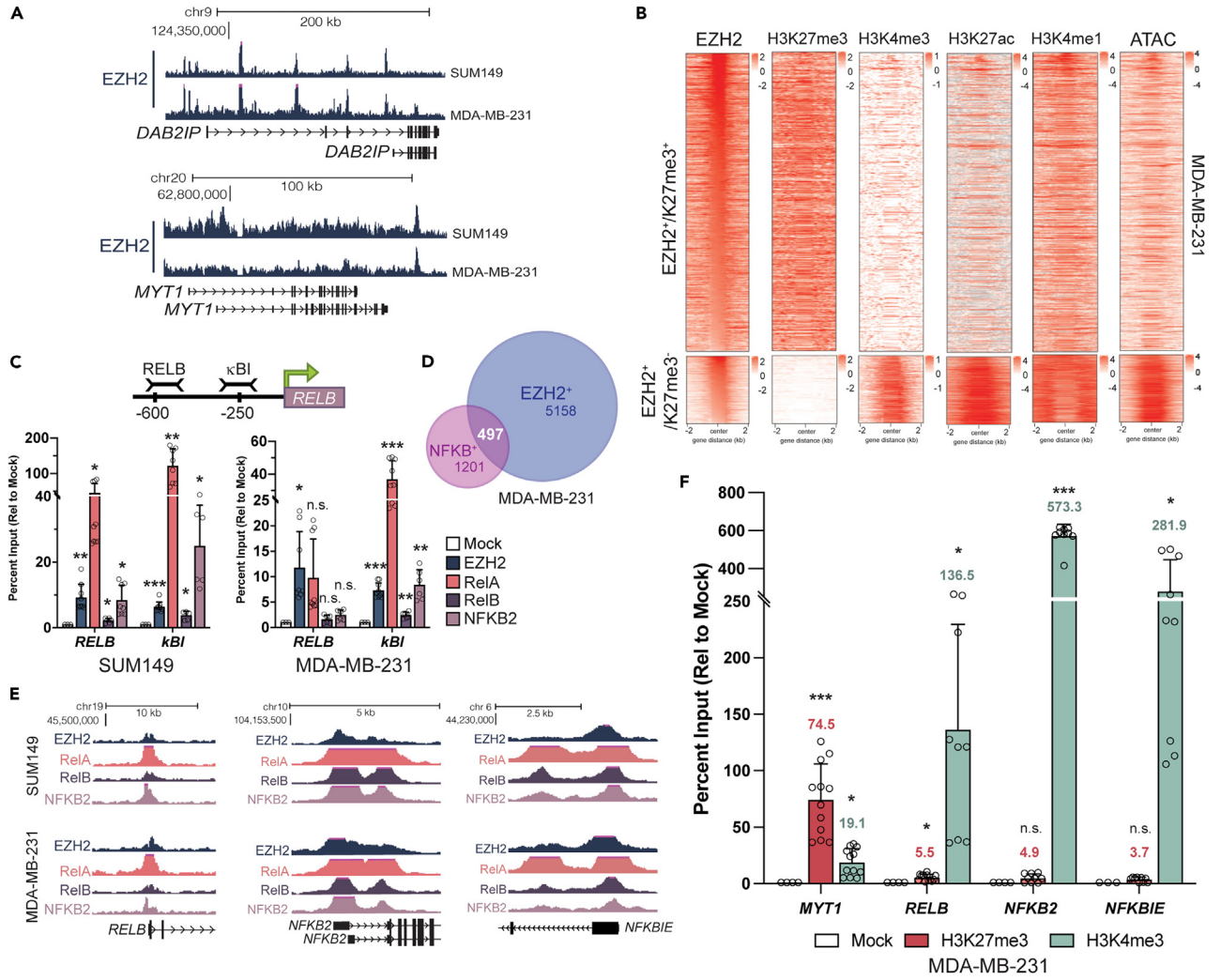

Figure 1. EZH2 colocalizes with NF-κB transcription factors at target genes in active chromatin

(A) EZH2 ChIP-seq tracks in SUM149 and MDA-MB-231 cells at canonical PRC2 target genes *DAB2IP* and *MYT1*.

(B) EZH2 ChIP-seq signal grouped by catalytic mark H3K27me3 presence or absence, further aligned with active H3K4me3, H3K27ac, and H3K4me1 histone mark ChIP-seq signals and ATAC-seq chromatin accessibility signal.

(C) EZH2 and NF-κB transcription factors RelA, RelB, and NFKB2 occupancy at two loci in the *RELB* promoter. Percent inputs represented relative to Mock IP.

(D) Overlap of EZH2 and RelA, RelB, and NFKB2 union ("NFKB") bound promoters (TSS +/− 5kb) in MDA-MB-231 cells.

(E) EZH2, RelA, RelB, and NFKB2 ChIP-seq tracks at promoters of NF-κB factor-encoding and target genes *RELB*, *NFKB2*, and *NFKBIE* in SUM149 and MDA-MB-231 cells.

(F) Repressive H3K27me3 and active H3K4me3 mark enrichment at *MYT1* and NF-κB target genes *RELB*, *NFKB2*, and *NFKBIE* in MDA-MB-231 cells. Percent inputs represented relative to Mock IP.

See also Figure S1, Tables S1 and S2. All quantification graphs are presented as mean ± SD. p values based on unpaired, two-tailed Student's *t* test assuming normal distribution as follows: *p < 0.05, **p < 0.01, ***p < 0.001, ****p < 0.0001, n.s. not significant.

previously published EZH2 binding site and a site containing an NF-κB binding motif ("kBI") in the *RELB* promoter, we indeed observed all factors bound to at least one locus in both cell lines (Figure 1C).[51] We next performed ChIP-seq to determine global promoter localizatation of unstimulated RelA, RelB, and NFKB2 and found 1691 and 2919 RelA$^+$, 19 and 156 RelB$^+$, and 59 and 3437 p52$^+$ promoters in MDA-MB-231 and SUM149 cells, respectively (Table S1, GEO: GSE223959). We observed a greater number of NFKB$^+$ genes in SUM149 compared to MDA-MB-231 cells; the SUM149 cell line is derived from inflammatory invasive ductal carcinoma and characterized as inflammatory, which may explain the higher presence of NF-κB factors on DNA.[68,69] Importantly, we found that our RelA-bound genes were common with about 56% (MDA-MB-231) and 69% (SUM149) of RelA-bound genes published in a 2020 ChIP-Seq study from Ngo

et al. which, considering differences in cell line (TNBC versus MEF) and conditions (unstimulated versus TNFα stimulation), we found to indicate biological agreement (Table S1).[70]

As there were relatively few RelB$^+$ and p52$^+$ promoters, the NF-κB factor bound-genes were combined into the union set "NFKB." We next determined which promoters were bound by both EZH2 and at least one NF-κB factor within NFKB (EZH2$^+$/NFKB$^+$) in MDA-MB-231 and SUM149 cells. Our ChIP-seq results indicated a subset of NF-κB bound genes were co-occupied by EZH2, including NF-κB factor-encoding and target genes, such as *RELB*, *NFKB2,* and *NFKBIE* (Figures 1D–1E, and S1D–S1E). ChIP-seq binding and co-occupation results were validated with ChIP-qPCR at canonical EZH2-PRC2 target genes *MYT1* and *DAB2IP*, and EZH2-NF-κB target genes *NFKBIE* (Figure S1G) in addition to *RELB* and *NFKB2* (Figures 1C, 4C, and 4E). We found EZH2$^+$/NFKB$^+$ genes enriched for HALLMARK signature "TNFa signaling via NF-κB" and other cancer-related signatures including "hypoxia" and "epithelial mesenchymal transition," as well as GO-slim biological process transcription signatures (Figure S1F). Further, RHD (p65 and p50/p52) motifs were among significantly enriched motifs colocalized by EZH2 and RelA (Figure S1H, Table S2).

We next compared the 5556 EZH2$^+$/H3K27me3$^-$ active chromatin sites with NFKB peaks and found 178 EZH2+/H3K27me3-sites overlapped at least one NF-κB transcription factor and 88 of the overlaps occured within 5kb of the TSS of a gene (Table S1). These 88 genes, including *NFKB2* and *NFKBIE*, constitute putative EZH2-NF-κB co-regulated genes and are enriched for the HALLMARK signature "TNFa signaling via NF-κB" (Figure S1I). Notably, 94 EZH2$^+$/NFKB$^+$ sites were also present in the H3K27me3$^+$ population; however, they represent a much lower proportion than the co-occupied genes in active chromatin (0.6% versus 3%). Since NF-κB transcription factor binding can be either activating or repressing, it is possible EZH2 and NF-κB may interact as corepressors in TNBC cells.[71] Finally, to validate our comparative analysis using public data we performed ChIP-qPCR for H3K27me3 and H3K4me3 at EZH2-NF-κB co-occupied genes. We observed enrichment of repressive H3K27me3 at canonical PRC2 target gene *MYT1*, and enrichment of active H3K4me3 at proposed activated target genes *RELB*, *NFKB2*, and *NFKBIE* in agreement with our *in silico* comparison (Figure 1F).

Together, we identified a subpopulation of EZH2 that binds genes in active regions of chromatin, and found EZH2 and NF-κB transcription factors co-occupy a subset of NF-κB and other cancer-related genes in TNBC cell lines.

EZH2 positively regulates expression of NF-κB genes including *RELB* and *NFKB2*

As EZH2 localized at NF-κB target genes in TNBC cells, we next asked whether EZH2 positively regulated the transcription of these genes. To accomplish this, we treated SUM149 and MDA-MB-231 cell lines with either non-targeting control or EZH2-targeting siRNA and performed RNA-seq. These experiments identified 3385 differentially expressed genes (DEGs) common between cell lines, approximately 16% of which had an absolute value log2 fold change in expression greater than 1 (Figure 2A, Table S3, GEO: GSE223959). With a well-established role as a gene silencer, we expected a loss of EZH2 to result in the majority of DEGs to be upregulated. Interestingly, we observed a similar number of up- and down-regulated DEGs in each cell line, which suggested EZH2 plays a substantial role as a positive regulator of gene expression in TNBC cells (Figure 2B). *RELB* was among the most highly decreased genes in both cell lines, and *NFKB2* and *NFKBIE* were downregulated in MDA-MB-231 cells. Beyond family members, we observed downregulation of NF-κB target genes including *IL6, CCND1*, and *SOX9* (Table S3).

To further assess genes positively regulated by EZH2, we considered only genes downregulated with EZH2 knockdown (siEZH2^{down}), of which there were 1598 common between SUM149 and MDA-MB-231 cells (Figure 2C). GSEA with HALLMARK sets revealed multiple cancer-related enrichments such as Myc target gene and cell cycle signatures, as well as "TNFa signaling via NF-kB" (Figure 2D). We next performed qPCR to validate EZH2 regulation of a panel of NF-κB target genes including *RELB*, *IL6, NFKB2, CCND1*, and *SOX9,* and found all were downregulated significantly in at least one cell line, while canonical target gene *DAB2IP* was upregulated in both cell lines following EZH2 knockdown (Figure 2E). Consistently, RelB protein levels were decreased while DAB2IP protein levels were increased following EZH2 knockdown (Figure 2F). RelA mRNA and protein levels remained unchanged, which suggests EZH2 is not regulating NF-κB genes indirectly via downregulation of RelA itself (Figure S2A). If EZH2 positively regulated expression of genes such as *RELB*, we expected a loss of target gene mRNA consistent with a loss of EZH2 protein, followed by a

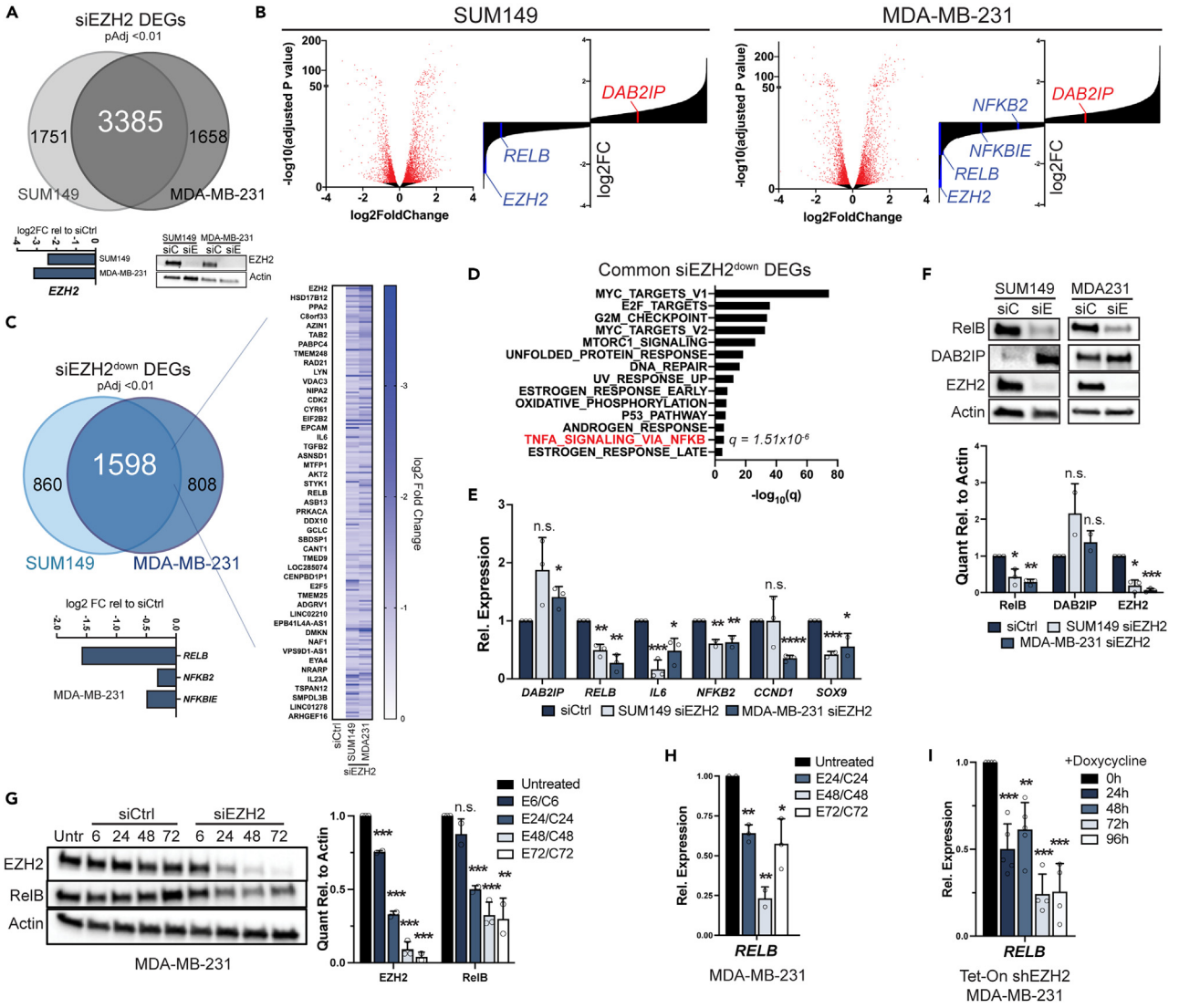

Figure 2. EZH2 is positively correlated with *RELB* and NF-κB genes

(A) 3385 common genes are differentially expressed (p_{Adj} < 0.01) following EZH2 knockdown in SUM149 and MDA-MB-231 cells as detected by RNA-seq. Validation of EZH2 knockdown at mRNA and protein level below.

(B) Up- and down-regulated gene counts following EZH2 knockdown in SUM149 and MDA-MB-231 cells. Red points on volcano plots indicate p_{Adj} < 0.01.

(C) 1598 common genes are differentially downregulated following EZH2 knockdown (siEZH2^{down}) in SUM149 and MDA-MB-231 cells (left), including NF-κB targets *RELB*, *NFKB2*, and *NFKBIE*, and heatmap visualzation of log2FC values for each cell line (right).

(D) GSEA of common siEZH2-down genes using HALLMARK signature database.

(E) mRNA levels of a panel of NF-κB target genes in both SUM149 and MDA-MB-231 cells following EZH2 knockdown for 48 h (siEZH2).

(F) Protein levels of RelB and DAB2IP in both SUM149 and MDA-MB-231 cells following 48h siEZH2.

(G) RelB protein levels following siEZH2 over a course of 6–72 h in MDA-MB-231 cells.

(H) *RELB* mRNA levels following siEZH2 over a course of 6–72 h in MDA-MB-231 cells.

(I) *RELB* mRNA levels following Induction of EZH2 knockdown in Tet-On shEZH2 MDA-MB-231 cells using doxycycline treatment from 0 to 96 h.

See also Figure S2 and Table S3. All quantification graphs are presented as mean ± SD. p values based on unpaired, two-tailed Student's *t* test assuming normal distribution as follows: *p < 0.05, **p < 0.01, ***p < 0.001, ****p < 0.0001, n.s. not significant.

decrease in target gene product. Thus, we aimed to assess the dynamics of *RELB* mRNA and protein levels following EZH2 knockdown across a series of time points. Relative to control treatment to normalize transfection-induced responses, 6 to 72 h of siEZH2 treatment decreased EZH2 mRNA and protein levels (Figures 2G, and S2B). Subsequent to decreased EZH2 protein levels, RelB mRNA and protein levels decrease up to 48 h of siEZH2 treatment, with re-expression beginning at 72 h (Figures 2G and 2H).[72] In

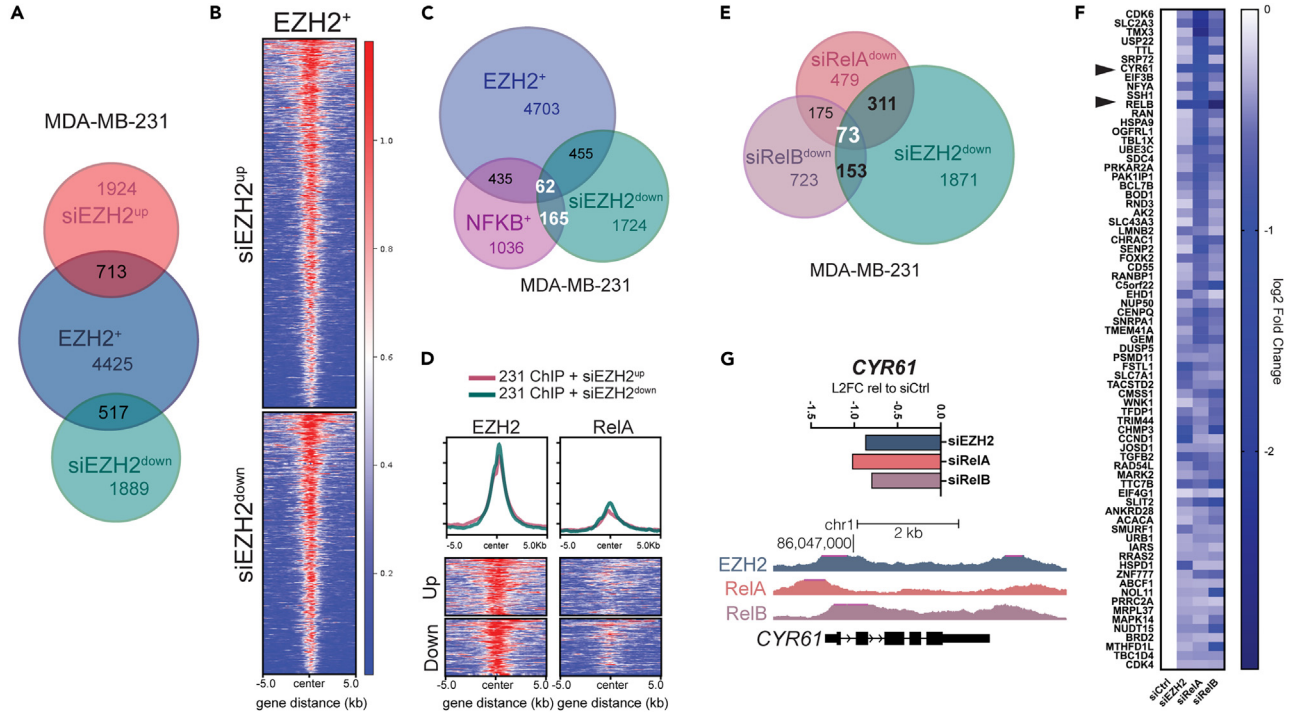

Figure 3. EZH2 co-occupies and co-activates a subset of NF-κB genes with RelA and RelB

(A) Overlap of EZH2-bound ($EZH2^+$) promoters with genes significantly ($p < 0.01$) up- or down-regulated by EZH2 knockdown ($siEZH2^{up/down}$) in MDA-MB-231 cells.

(B) $EZH2^+$ promoter (TSS +/− 5kb) ChIP-seq signal centered on TSS, sorted by $siEZH2^{up}$ (top) or $siEZH2^{down}$ (bottom) genes.

(C) Overlap of $EZH2^+$ and $NFKB^+$ promoters with $siEZH2^{down}$ genes.

(D) Traces of $EZH2^+$ or $RelA^+$ ChIP-seq signal intensity at $siEZH2^{up}$ (red) or $siEZH2^{down}$ (green) genes (topmost shown in heatmap, all signal integrated in trace).

(E) Overlap of $siRelA^{down}$, $siRelB^{down}$, and $siEZH2^{down}$ ($p < 0.01$) genes in MDA-MB-231 cells.

(F) Heatmap of log_2FC for common $siRelA^{down}$/$siRelB^{down}$/$siEZH2^{down}$ genes; *RELB* and *CYR61/CCN1* indicated by arrows.

(G) Log_2FC of *CYR61/CCN1* mRNA following EZH2, RelA, and RelB knockdown (left) and EZH2, RelA, and RelB ChIP-seq tracks at the *CYR61/CCN1* locus (right).

See also Figure S3 and Tables S3–S4.

addition to transient silencing, we utilized a stable, doxycycline-inducible 3'UTR-targeting shEZH2 system established in MDA-MB-231 cells (Figure S2C). Upon the addition of doxycycline, we found *RELB* mRNA and, to a lesser degree, protein levels decrease over time (Figures 2I, and S2C).

In all, we found EZH2 positively regulated expression of hundreds of genes in TNBC cell lines, including NF-κB factor-encoding and target genes, and cancer-related genes.

EZH2 coordinates with RelA and with RelB to positively regulate a subset of NF-κB target genes

We next integrated our ChIP-seq and RNA-seq datasets to define an EZH2-NF-κB co-activated gene signature using MDA-MB-231 cells, as we detected a greater number of EZH2 ChIP-seq peaks compared to SUM149 cells (Figure S1D). We compared genes bound by EZH2 ($EZH2^+$) with genes differentially expressed following EZH2 knockdown ($siEZH2^{up/down}$) and identified 713 $EZH2^+$/$siEZH2^{up}$ and 517 $EZH2^+$/$siEZH2^{down}$ genes (Figure 3A, Table S3). $EZH2^+$/$siEZH2^{down}$ genes were enriched for "TNFa signaling via NF-κB" and other cancer-related gene signatures such "cell cycle" (Figure S3A). We then plotted EZH2 ChIP-seq peak signal from −5kb to +5kb centered on each TSS for bound and DEGs (Figure 3B). EZH2 signal intensity appeared similar between up- and down-regulated genes, with perhaps more spreading on upregulated genes which may be expected as PRC2 spreads on heterochromatin.[73] To determine whether NF-κB factor binding was enriched at EZH2-activated genes, we first overlapped $NFKB^+$ genes against $EZH2^+$ and $siEZH2^{down}$ genes (Figure 3C, Table S3). NF-κB factors localized to genes activated

by EZH2 (62 EZH2^{+}/NFKB^{+}/siEZH2^{down} genes), but also siEZH2-downregulated genes lacking EZH2 binding (165 NFKB^{+}/siEZH2^{down} genes). Interestingly, both sets of genes were most highly enriched for "TNFa signaling via NF-κB" indicating a potential indirect regulatory link between EZH2 and NF-κB in addition to direct gene activation (Figures S3B–S3C). We next aligned RelA, RelB, and p52 ChIP-seq peaks against the same groups of EZH2^{+}/siEZH2$^{up/down}$ genes to visualize co-localization at DEGs. Overall, RelA, RelB, and p52 had less signal than EZH2 at EZH2-regulated genes, but RelA still had appreciable signal for the topmost EZH2-bound genes (Figures 3D, and S3D). Finally, when comparing EZH2^{+}/NFKB^{+}/siEZH2^{down} and EZH2^{+}/NFKB^{+}/H3K27me3^{-} derived putative co-activated genes, we found an overlap of 19 genes including *NFKB2* and *NFKBIE,* as well as genes with reported roles in breast cancer pathophysiology such as *SDC4* (Figures S3E–S3F, Tables S1, and S3).[74–76]

To more directly assess commonly activated genes, we silenced RelA and RelB, followed by RNA-seq and integration with the EZH2-regulated cistrome in MDA-MB-231 cells (Table S4, GEO: GSE223959). Comparing all downregulated genes, we found 73 siEZH2^{down}/siRelA^{down}/siRelB^{down} genes (Figures 3E and 3F, Table S4). These genes were enriched for NF-κB, Myc, and cell cycle signatures, similar to all siEZH2^{down} genes (Figure S3G). Further, EZH2 binding was associated with 129 siRelA^{down}, 170 siRelB^{down}, and 31 siRelA^{down}/siRelB^{down} DEGs (Figure S3H, Table S4). Of these co-activated genes, *CYR61* was confidently determined to both be bound by EZH2, RelA, and RelB and downregulated upon silencing of each factor (Figure 3G). *CYR61*, also known as *CCN1,* is a secreted extracellular matrix protein reported to promote breast tumorigenesis and contribute to aggressive TNBC/BLBC phenotypes.[54,55] Over 90% of siEZH2^{down}/siRelA^{down}/siRelB^{down} genes were bound by at least EZH2, and about 40% were co-occupied by EZH2 and RelA including *SMURF1,* which is involved in breast cancer cell migration and invasion, and *TRIM44,* which is an NF-κB modulator and poor prognostic factor in breast cancer patients (Figure S3I).[77,78]

In integrating genome-wide binding and transcriptomic data, we found that EZH2 and NF-κB factors both co-occupied and co-activated a subset of genes characterized by NF-κB signaling and other cancer-related signatures in TNBC cells.

EZH2 cooperates with RelA to increase NF-κB target gene expression and promoter localization

Following evidence of promoter occupation and positive regulation of genes, we next aimed to demonstrate direct transcriptional activation by EZH2. Transient overexpression of EZH2 with two separate constructs, pCDNA-FLAG-EZH2 and pCDH-HA-EZH2, increased RelB and NFKB2 mRNA and protein levels at 48 h in both SUM149 and MDA-MB-231 cells (Figures 4A–4B, and S4A–S4C). Closer examination of EZH2 overexpression over a timecourse of 0–72 h revealed increases in both RelB and NFKB2 mRNA levels following increases in EZH2 expression (S4D). Corresponding with increases in mRNA, transient overexpression increased EZH2 occupation of the *RELB* and *NFKB2,* as well as *MYT1* promoters in MDA-MB-231 cells (Figures 4C, and S4E). As we found EZH2 co-occupied and co-activated a subset of NF-κB genes with RelA, we utilized luciferase reporter plasmids driven by either a κB response element, or the entire 1.7kb *RELB* promoter region to directly assess cooperativity.[65,79] EZH2 overexpression induces a modest increase in NF-κB and *RELB* reporter activity over reporter alone in HEK293T cells, while RelA overexpression increases reporter activity substantially. EZH2 and RelA co-expression resulted in the highest reporter activity which suggest EZH2 and RelA cooperate to activate NF-κB genes such as *RELB* (Figure 4D). To assess co-recruitment dynamics to the *RELB* promoter, we silenced either EZH2 or RelA and performed ChIP-qPCR. We found EZH2 knockdown did not influence the presence of RelA, RelB, or NFKB2 at the *RELB* promoter (Figure S4F). Interestingly, RelA knockdown reduced EZH2 presence at the *RELB* and *NFKB2* but not *MYT1* promoters suggesting RelA is important for the localization of EZH2 to non-canonical NF-κB gene loci (Figures 4E, and S4G).

We next asked whether EZH2 and RelA cooperate via physical interaction. Endogenous immunoprecipitation of EZH2 from MDA-MB-231 lysates revealed expected interactions with EED, as well as interactions with RelA (Figure 4F). Reciprocally, immunoprecipitation of RelA revealed EZH2 but not EED interactions, indicating this is a PRC2-independent interaction (Figure 4G). Supporting a physical interaction is indeed formed between EZH2 and RelA endogenously in TNBC cells, treatment of MDA-MB-231 cells with EZH2-targeting proteolysis-targeting chimera (PROTAC) MS177 decreased the protein levels of RelA in a dose-dependent manner corresponding with EZH2 protein loss (Figure 4H). Interestingly, RelB protein

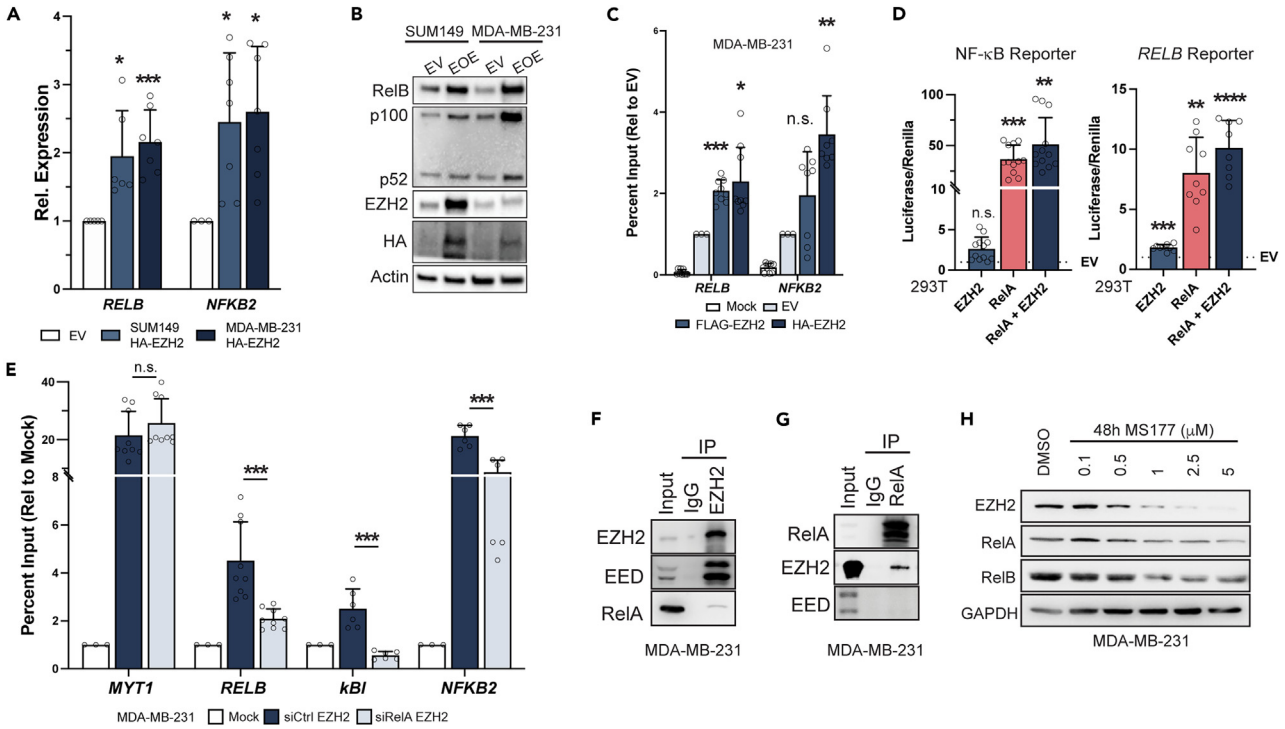

Figure 4. EZH2 promotes the expression of *RELB* and *NFKB2* cooperatively with RelA

(A) *RELB* and *NFKB2* mRNA levels following 48 h EZH2 overexpression with HA-EZH2 construct normalized to empty vector (EV) in SUM149 and MDA-MB-231 cells.

(B) RELB and *NFKB2* gene product p100 protein levels following 48 h EV or EZH2 overexpression using HA-EZH2 construct in SUM149 and MDA-MB-231 cells.

(C) EZH2 occupancy of *RELB* and *NFKB2* promoters following 48 h EZH2 overexpression using FLAG-EZH2 and HA-EZH2 constructs, normalized to EV conditions, in MDA-MB-231 cells.

(D) Renilla-normalized luciferase signal generated from NF-κB response element reporter or *RELB* promoter reporter in HEK293T cells co-expressed with EZH2, RelA, or RelA + EZH2.

(E) EZH2 occupancy of two loci in the *RELB* promoter and the *NFKB2* promoter before (dark blue) and after (light blue) RelA knockdown in MDA-MB-231 cells. Percent inputs represented relative to Mock IP.

(F) Immunoprecipitation of endogenous EZH2 from MDA-MB-231 cells and immunoblotting for EZH2, PRC2 subunit EED, and RelA.

(G) Immunoprecipitation of endogenous RelA from MDA-MB-231 cells and immunoblotting for RelA, EZH2, and PRC2 subunit EED.

(H) EZH2, RelA, and RelB protein levels following treatment with 48 h EZH2 PROTAC MS177 from 0.1 to 5μM in MDA-MB-231 cells.

See also Figure S4. All quantification graphs are presented as mean ± SD. p values based on unpaired, two-tailed Student's *t* test assuming normal distribution as follows: *p < 0.05, **p < 0.01, ***p < 0.001, ****p < 0.0001, n.s. not significant.

additionally decreased upon MS177 treatment which supports our proposed positive relationship between EZH2 and RelB, and further is in agreement with previous reports of a trimeric EZH2-RelA-RelB complex.[30]

EZH2 interacts with RelA via its transactivation domain to activate *RELB* and *NFKB2* and promote malignant phenotypes

Following recent reports of an EZH2 transactivation domain (TAD) that facilitates transcriptional activity and co-activator interactions, we aimed to determine whether this domain facilitates interactions with RelA.[31,52] Indeed, a GST-EZH2 (135–200) construct containing the TAD was sufficient to pull down RelA *in vitro* (Figure 5A). When two critical residues for transcriptional activity (F171/F145) are mutated to alanine, lysine, or a combination, the *in vitro* interactions between the EZH2-TAD construct and both RelA and RelB are lost, suggesting the functional TAD mediates EZH2-RelA/RelB interactions (Figure 5B). Indeed, RelA is more efficiently co-precipitated with WT EZH2 compared to mutant TAD EZH2 when co-expressed in HEK293T cells, and we found that RelA co-precipitated with reconstituted WT but not mutant TAD EZH2 when expressed in MDA-MB-231 cells depleted of endogenous EZH2 (Figures 5C, and S5A).

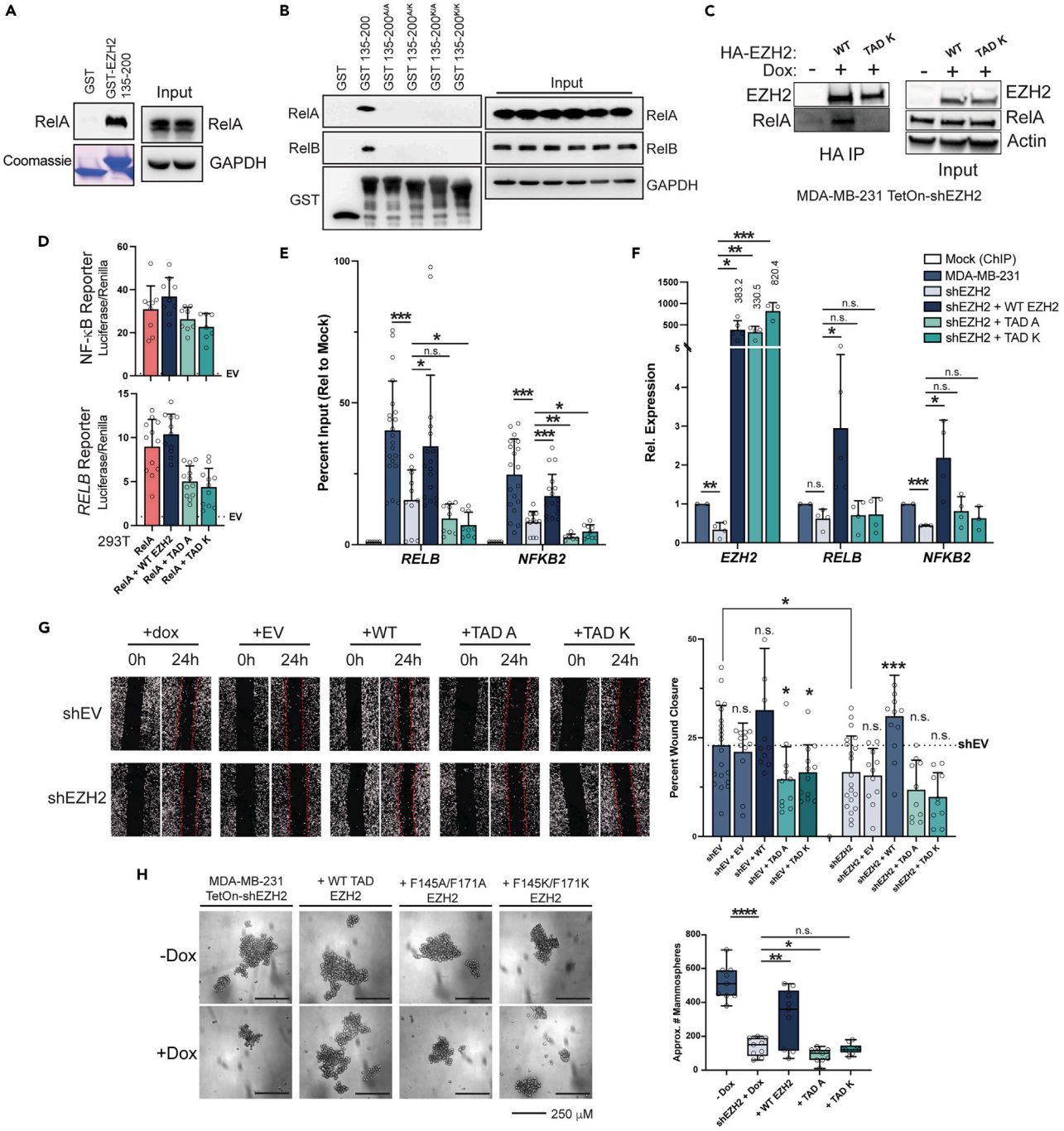

Figure 5. EZH2 physically interacts with RelA and RelB via transactivation domain to activate *RELB* and *NFKB2* and promote malignant phenotypes

(A) *In vitro* pulldown of GST-EZH2 (135–200) containing the TAD and immunoblotting for RelA. Coomassie stain indicating loading of GST and GST-EZH2.

(B) *In vitro* pulldown of GST-EZH2 (135–200) or constructs with mutations to critical TAD residues (F171A/F145A, F171A/F145K, F171K/F145A, F171K/F145K) and immunoblotting for RelA and RelB.

(C) HA-conjugated bead pulldown from doxycycline-induced MDA-MB-231 shEZH2 Tet-On cells with no, WT, or TAD K (F171K/F145K) HA-EZH2 reconstitution, followed by immunoblotting for EZH2 and RelA.

(D) Renilla-normalized luciferase signal generated from NF-κB response element reporter or *RELB* promoter reporter in HEK293T cells co-expressing RelA with WT EZH2 or mutant TAD EZH2 (TAD A: F171A/F145A; TAD K: F171K/F145K) (dotted line indicates EV background luciferase signal).

(E) EZH2 occupancy of *RELB* and *NFKB2* promoters in MDA-MB-231 shEZH2 Tet-On cells without induction, with 48 h doxycycline shEZH2 induction, or with 48 h doxycycline shEZH2 induction plus 24 h WT or mutant TAD EZH2 expression. Percent inputs represented relative to Mock IP.

Figure 5. *Continued*

(F) *EZH2, RELB,* and *NFKB2* mRNA levels in MDA-MB-231 shEZH2 Tet-On cells without induction, with 48 h doxycycline shEZH2 induction, or with 48 h doxycycline shEZH2 induction plus 24 h WT or mutant TAD EZH2 expression.

(G) Migration at 0h and 24 h post-scratch wound of MDA-MB-231 shEV or shEZH2 Tet-On cells with 48 h doxycycline treatment alone, or 48 h doxycycline plus 48 h EV, WT EZH2, or mutant TAD EZH2 expression pre-wound (quantified as percent wound closure, right).

(H) Mammospheres after 7 days of non-adherent growth of MDA-MB-231 shEZH2 Tet-On cells without or with 48 h doxycycline shEZH2 induction (left), or MDA-MB-231 shEZH2 Tet-On cells additionally stably expressing WT or mutant TAD EZH2 without or with 48 h doxycycline shEZH2 induction (right three) (quantified as approximate number of mammospheres, right).

See also Figure S5. All quantification graphs are presented as mean ± SD. p values based on unpaired, two-tailed Student's *t* test assuming normal distribution as follows: *p < 0.05, **p < 0.01, ***p < 0.001, ****p < 0.0001, n.s. not significant.

We next assessed the requirement of the functional TAD for transcriptional co-activation and contribution to cancer cell phenotypes by EZH2 and RelA. Contrary to our previous findings with WT EZH2, we found mutant TAD EZH2 did not increase NF-κB and *RELB* reporter signal co-operatively with RelA (Figures 5D,and 4D). Further, following induction of shEZH2 in MDA-MB-231 cells with a corresponding loss of EZH2 localization and target gene expression, we found WT EZH2 reconstitution could rescue both localization to the *RELB* and *NFKB2* promoters and activation of gene expression to a greater degree than TAD mutant EZH2, whereas localization rescue levels are similar between WT and mutant EZH2 at the *MYT1* promoter (Figures 5E–5F, and S5B–S5C). As NF-κB signaling and EZH2 are both independently reported to contribute to malignant characteristics, such as motility and stemness in TNBC cells, we next assessed whether the TAD linking EZH2 with RelA was required for these phenotypes. We found only WT but not mutant TAD could promote and rescue migration and non-adherent growth of MDA-MB-231 cells (Figures 5G and 5H). Together, these data suggest that the TAD of EZH2, required for efficient physical interaction with RelA, is important for non-canonical promoter localization, gene expression, and downstream malignant phenotype contributions in TNBC cells.

EZH2 activation of NF-κB and promotion of malignant phenotypes is PRC2-independent

Although RelA immunoprecipitation revealed no EED interaction (Figure 4G), we nonetheless desired to evaluate whether EZH2 activation of *RELB* and downstream promotion of malignant phenotypes is independent of PRC2. Indeed, contrary to EZH2 knockdown, knockdown of SUZ12 and EED, PRC2 degradation with EED-targeting PROTAC UNC6852, and EZH2 catalytic inhibition with GSK126 and Tazemetostat all failed to decrease *RELB* mRNA levels (Figure 6A). Further, RelB protein levels were not decreased with PRC2 component knockdown or degradation (Figure 6B). Further comparison of UNC6852 to EZH2-targeting PROTAC MS177 revealed that while UNC6852 dose-dependently decreased EZH2/EED but not RelA/RelB protein levels, MS177 decreased both EZH2/EED and RelA/RelB protein levels (Figure 6C). Catalytic inhibition of EZH2 with C24 did not alter levels of RelA or RelB protein and, downstream, we found that MS177 decreased colony formation capability of MDA-MB-231 cells to a greater degree than catalytic inhibition alone (Figure 6D). Finally, MDA-MB-231 cells pre-treated with either UNC6852, siEZH2, or MS177 were subjected to non-adherent growth conditions. PRC2-targeting with UNC6852 did not significantly impact mammosphere formation, while both siEZH2 and MS177 treatment significantly decreased both mammosphere size and number (Figure 6E). Interestingly, GSK126 treatment was also found to decrease sphere size and number, which is in agreement with reported contributions of EZH2 catalytic activity to oncogenic TNBC phenotypes (Figure S6A).[35,51] However, GSK126 treatment did not alter RELB expression nor EZH2 occupation of the RELB promoter, supporting HMT-independent NF-κB activation (Figures 6A and S6B). Taken together, these results indicate a PRC2-independent function for EZH2 important for *RELB* activation and downstream malignant phenotypes.

The EZH2-NF-κB activation signature is enriched in TNBC/BLBC patients

Finally, we assessed whether EZH2-NF-κB co-activated genes are preferentially expressed in human TNBC patients. Utilizing the METABRIC and TCGA databases accessed via cBioPortal, we first evaluated *EZH2* and *RELB* expression levels in samples categorized either by estrogen receptor (ER) status or molecular subtyping as defined by PAM50 plus claudin-low classification, where the basal-like subtype highly overlaps with hormone receptor-categorized TNBC, and both ER-negative and basal-like cases are more aggressive with a worse prognosis compared to other subtypes.[80–85] We found *EZH2* and *RELB* mRNA levels were elevated in ER-negative and basal-like patient samples compared to other subtypes from both METABRIC and TCGA databases (Figure 7A). Interestingly, *SUZ12* and *EED* mRNA levels were not elevated over other subtypes in the same ER-negative and basal-like cases, supporting the proposed PRC2-independent role of EZH2 in these subtypes of breast cancer (Figure S7A). We next stratified patient

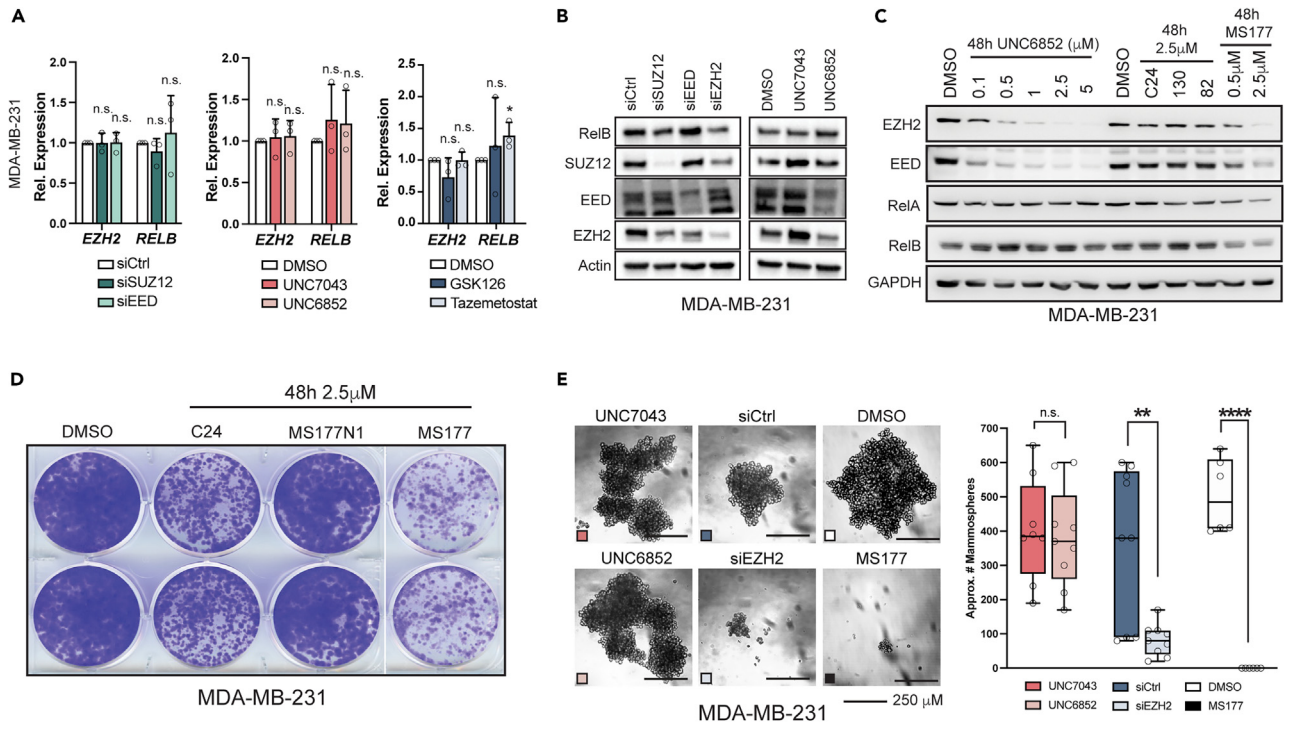

Figure 6. EZH2 activates *RELB* and promotes malignant phenotypes independently of PRC2

(A) *EZH2* and *RELB* mRNA levels following siRNA-mediated knockdown of PRC2 subunits SUZ12 or EED (left), EED-targeting PROTAC UNC6852 degradation (center, compared to inactive control compound UNC7043; dose 6.25μM), or 5μM GSK126 or 0.5μM Tazemetostat treatment (right).

(B) RelB, SUZ12, EED, and EZH2 protein levels following siRNA-mediated knockdown of PRC2 subunits SUZ12 or EED, or EED-targeting PROTAC UNC6852 degradation (compared to inactive control compound UNC7043; dose 6.25μM).

(C) RelB, RelA, EZH2, SUZ12, and EED protein levels following 48 h UNC6852 treatment (left lanes) compared to 48 h EZH2 PROTAC MS177 treatment (rightmost two lanes), further compared to 48 h catalytic EZH2 inhibitor C24, and MS177 control compounds "130" and "82" (center lanes).

(D) Colony formation capacity of MDA-MB-231 cells following 48 h catalytic inhibitor C24 treatment compared to 48 h treatment with inactive MS177N1 or active MS177 compounds (2.5μM).

(E) Mammospheres after 7 days of non-adherent growth of MDA-MB-231 cells treated at the time of plating with EED PROTAC (UNC7043 vs. UNC6852; 6.25μM), EZH2 knockdown (siCtrl vs. siEZH2), or EZH2 PROTAC (DMSO vs. MS177; 2.5μM) (quantified as approximate number of mammospheres, right).

See also Figure S6. All quantification graphs are presented as mean ± SD. p values based on unpaired, two-tailed Student's *t* test assuming normal distribution as follows: *p < 0.05, **p < 0.01, ***p < 0.001, ****p < 0.0001, n.s. not significant.

samples into quartiles by *EZH2* or *RELB* mRNA level, then grouped cases with common *EZH2* + *RELB* quartile rankings such that the "*EZH2* + *RELB* mRNA 4th quartile" group represents those patients within the top quartile for both *EZH2* and *RELB* (Table S5). Following this stratification, we found patient samples with the highest levels of *EZH2* and *RELB* mRNA constituted a higher percentage of ER-negative or basal-like samples compared to those with the lowest levels of *EZH2* and *RELB* mRNA (Figure 7B). Additionally, the METABRIC *EZH2* + *RELB* 4th quartile cases had higher Nottingham Prognostic Indices, represented a higher percentage of neoplasm histologic grade 3 samples, and constituted a higher percentage of patients who received chemotherapy compared to *EZH2* + *RELB* 1st quartile case (Figure S7B). Further, *EZH2* and *RELB* mRNA levels were positively correlated in both ER-negative and basal-like + claudin-low samples, while there is no significant correlation in ER-positive or luminal-like + HER2 samples from the METABRIC dataset (Figure 7C). Finally, we assessed expression of the EZH2 and RelA co-activated genes ($EZH2^{+}/RelA^{+}/siEZH2^{down}$) in both datasets and found these genes tended to have higher expression levels in basal-like samples compared to other subtypes, with some genes also highly expressed in claudin-low subtype samples (Figure 7D). $EZH2^{+}/RelA^{+}/siEZH2^{down}$ genes with elevated mRNA levels in basal-like and claudin-low subtypes exhibited corresponding elevated protein levels in patient samples from the Clinical Proteomic Tumor Analysis Consortium (CPTAC) breast cancer proteogenomic landscape database (Figure S7C).[86] Further, beyond elevation in basal-like and claudin-low subtypes compared to other BC subtypes, these genes additionally appear elevated over other types of cancer profiled in the TCGA PanCancer Atlas again highlighting the influence of cellular context on non-canonical EZH2 (Figure S7D).[87]

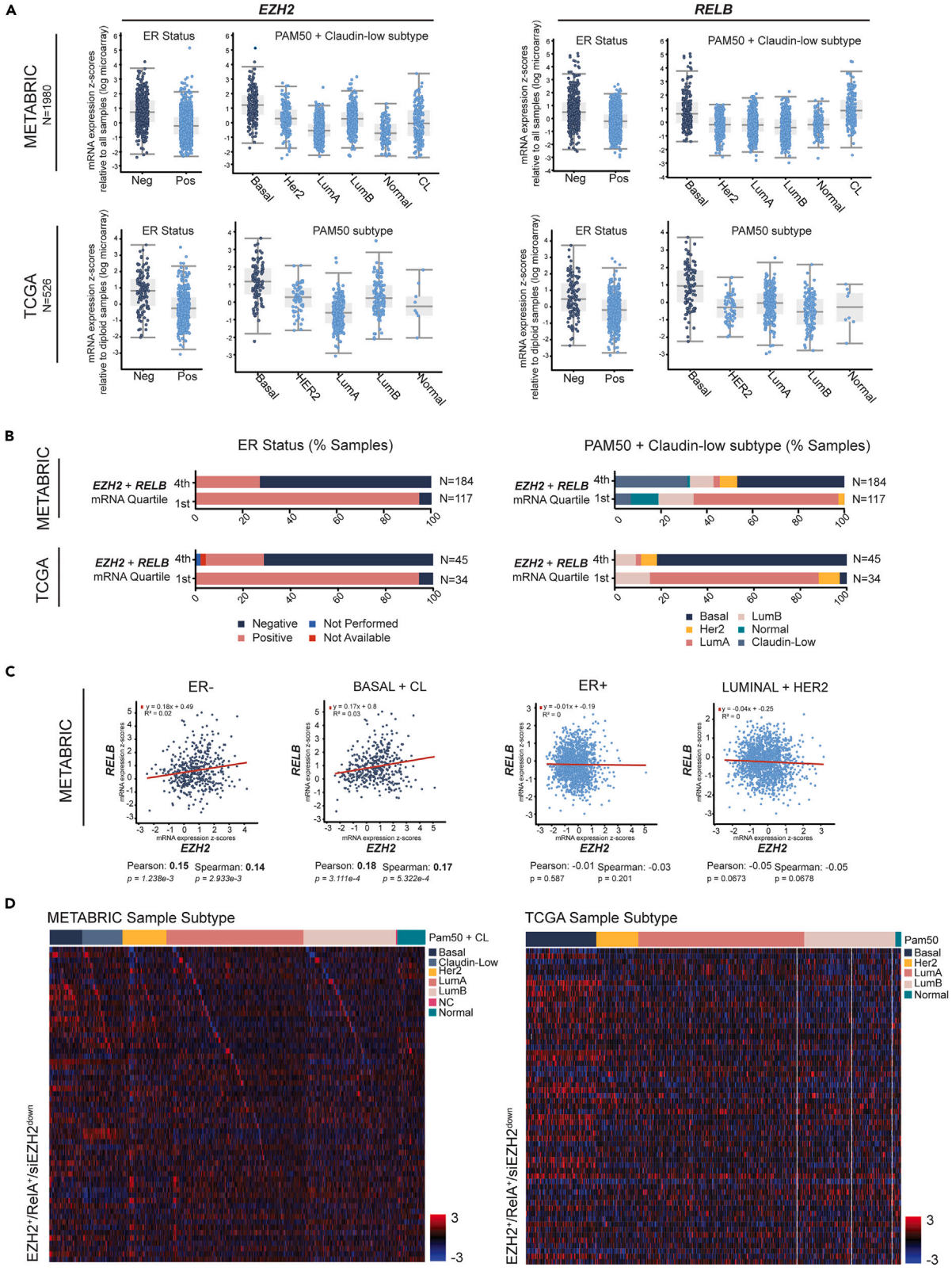
A
EZH2
RELB
METABRIC
N=1980
TCGA
N=526
ER Status
PAM50 + Claudin-low subtype
PAM50 subtype
mRNA expression z-scores relative to all samples (log microarray)
mRNA expression z-scores relative to diploid samples (log microarray)
Neg
Pos
Basal
Her2
LumA
LumB
Normal
CL
B
ER Status (% Samples)
PAM50 + Claudin-low subtype (% Samples)
EZH2 + RELB mRNA Quartile
4th
1st
N=184
N=117
N=45
N=34
Negative
Positive
Not Performed
Not Available
Basal
Her2
LumA
LumB
Normal
Claudin-Low
C
ER-
BASAL + CL
ER+
LUMINAL + HER2
RELB
EZH2
Pearson: 0.15 Spearman: 0.14
p = 1.238e-3 p = 2.933e-3
Pearson: 0.18 Spearman: 0.17
p = 3.111e-4 p = 5.322e-4
Pearson: -0.01 Spearman: -0.03
p = 0.587 p = 0.201
Pearson: -0.05 Spearman: -0.05
p = 0.0673 p = 0.0678
D
METABRIC Sample Subtype
TCGA Sample Subtype
Pam50 + CL
Pam50
Basal
Claudin-Low
Her2
LumA
LumB
NC
Normal
EZH2+/RelA+/siEZH2down
3
-3

Figure 7. *EZH2* and *RELB* are highly expressed and positively correlated in aggressive breast cancer subtypes

(A) mRNA expression z-scores of *EZH2* (left) and *RELB* (right) in different breast cancer subtypes (Estrogen Receptor (ER) status or PAM50 + Claudin-low) from patients in both the METABRIC (top) and TCGA (bottom) databases. ER-negative and basal-like samples indicated in dark blue.

(B) Fourth and first quartiles of patient samples sorted by *EZH2* and *RELB* mRNA z-scores (4^{th} quartile = both high *EZH2* and *RELB* mRNA; 1^{st} = both low *EZH2* and *RELB* mRNA) were identified and further classified by ER status (left) and PAM50 + Claudin-low subtype (right) for both METABRIC (top) and TCGA (bottom) datasets.

(C) Correlation between *EZH2* and *RELB* mRNA z-scores in either ER-negative and basal-like/claudin-low (left, dark blue) or ER-positive and luminal/HER2 (right, light blue) patient samples from the METABRIC dataset. Pearson and Spearman correlation values and p values calculated on cBioPortal and reported per correlation graph.

(D) Expression of $EZH2^{+}$/$RelA^{+}$/$siEZH2^{down}$ genes queried in both the METABRIC (left) and TCGA (right) datasets and sorted by PAM50 + claudin-low subtype.

See also Figure S7 and Table S5.

Together, we found *EZH2*, *RELB*, and EZH2-RelA activated genes were more highly expressed and correlated in ER-negative and basal-like subtype patient samples, highlighting the clinical relevance of this non-canonical EZH2 signaling axis in more aggressive subsets of breast cancer.

DISCUSSION

Our study demonstrates PRC2-independent EZH2 transcriptional activation of a subset of NF-κB target genes in coordination with RelA, RelB, and NFKB2 in TNBC cells. It was previously reported that EZH2 interacted with RelA and RelB to activate NF-κB signaling.[30] Here, we expand on these findings by integrating global promoter binding of EZH2 and NF-κB transcription factors with transcriptomic changes following depletion of those factors to profile the EZH2-NF-κB co-activation signature in TNBC cells. This allows us to define a specific NF-κB target gene signature positively regulated by EZH2, and provide broader insights into the activating role of EZH2 in TNBC cells. Our genomic profile provides valuable NF-κB binding data, especially under unstimulated conditions in disease context, and considering subunits beyond RelA, and further provides a foundation for inquiries into additional oncogenic EZH2 gene activation implications in TNBC cells. Beyond NF-κB, we found EZH2-bound genes enriched for cancer-related signatures including EMT and hypoxia, and positively regulated the transcription of genes enriched for Myc target gene, cell cycle, and DNA repair signatures. We believe future studies interrogating EZH2-RelA contributions to EMT, cell cycle, and other oncogenic processes, as well as exploring how EZH2 may promote these phenotypes with co-activators beyond NF-κB transcription factors, would provide valuable insights into TNBC cell signaling for therapeutic approach development.

We demonstrate EZH2 transcriptionally activates the genes encoding RelB (*RELB*) and p100 (*NFKB2*), which is proteolytically cleaved to transcription factor p52. The canonical NF-κB signaling pathway functions largely through RelA, while RelB and p52 constitute the non-canonical arm of NF-κB signaling. Beyond different transcription factors, each signaling arm also has differing stimuli, mechanisms of activation, target genes, and biological associations.[67,88] It is possible that EZH2, by activating *RELB* and *NFKB2*, increases the presence and activity of RelB-p52 heterodimers. This, along with co-activation with RelA, may contribute to chronic NF-κB activation and complex inflammatory signaling in TNBC.[43,46] The specific role of RelB downstream of EZH2 activation, and in its own activation, remains unclear. In addition to EZH2 and RelA cooperatively activating *RELB*, we found RelB could be pulled down with EZH2 along with RelA; interestingly, RelA has been reported to dampen RelB activity, and RelA-RelB heterodimers, although infrequently described, have been reported to be transcriptionally inactive.[89,90] We speculate the presence of EZH2 may be necessary for the observed transcriptional activity of this trimeric complex, and that the cellular context may permit gene activation. The dynamics of this complex and how it may contribute to a feedforward non-canonical NF-κB signaling loop of RelB activating *RELB* and *NFKB2* expression that may aberrantly activate downstream immunity and inflammatory pathways,[91] merits future study.

We additionally expand on the functional relationship between EZH2 and RelA. Not only do EZH2 and RelA physically interact, depletion of RelA diminishes EZH2 localization at non-canonical promoters suggesting a role in chromatin recruitment and gene targeting. Activation of these genes appears strongest when both RelA and EZH2 are present, yet the specific function of EZH2 in this gene activation remains unclear. In prior studies, EZH2 was suggested to interact with histone acetyltransferase p300, SWI/SNF, and RNA Pol II to form a transcriptional activation complex.[31,52] From this, we can speculate that a generic activation complex including EZH2 and p300 is recruited to specific target genes by factors like RelA, and that this specification would likely be cancer cell context-dependent. This question and the specific role and

requirement of EZH2 in this transcriptional activation complex and downstream oncogenic impacts warrant future study.

Reconciling our findings of EZH2 gene activation with well-established canonical gene repression, we describe a mechanism by which EZH2 may promote transcription via its transactivation domain (TAD). As recently reported, the typically buried TAD appears to structurally unlock in cancer contexts and allow EZH2 to form non-PRC2 protein interactions, such as with Myc, AR, and as described here, RelA.[31,52,53] Beyond mediating the physical interaction between EZH2 and RelA, we demonstrate a functional TAD is required for EZH2 and RelA co-activation of *RELB* and *NFKB2,* including EZH2 localization to these promoters and activation of their expression. Further exploration of the TNBC context-specific signals that "unlock" the EZH2 TAD and allow for RelA interaction and downstream co-activation is warranted. Residue S21 of EZH2 is reported to be a site of cancer-specific phosphorylation by AKT, and this modification is reported to make the TAD structurally available, as well as possibly serving as a "functional switch" away from canonical PRC2 activity and contributing to non-canonical EZH2 activity in multiple types of cancer including glioblastoma multiforme, CRPC, and breast cancer.[28,33,92,93] We speculate phosphorylation at this site in TNBC cells would reveal the TAD and subsequently allow EZH2 to form physical interactions with non-PRC2 co-activators including RelA, which could then recruit EZH2 to target genes for transcriptional activation.

Multiple variations of "non-canonical" EZH2 activity have been reported in breast and other cancers, differing in details such as PRC2-independence and HMT-independence, which are well summarized in recent reviews.[27,94] Using both RNA interference and chemical degrader approaches, we demonstrate EZH2 activation of target gene *RELB* does not require PRC2 subunits SUZ12 and EED. EZH2-NF-κB activation also appears HMT-independent as EZH2 inhibition does not mimic knockdown, and approximately 25% of EZH2 sites including NF-κB activated targets are not coincident with H3K27me3. Other studies have reported EZH2 "solo" sites that are similarly devoid of PRC2 or H3K27me3, but we believe there may be more complexity involved. As reported in a 2021 study in CRPC analyzing AR-bound genes, it was found that although EZH2 bound these genes at the highest frequency, subcomplexes of EZH2-SUZ12, EZH2-EED, and the entire PRC2 core complex were present at notable frequencies.[32] Indeed, alterations in PRC2 subcomplex combinations as mediated by GATA factors has been reported to mediate non-canonical functions.[95] We believe further ChIP-seq analysis of PRC2 subunits in comparison with our EZH2 and NF-κB binding data may reveal similar groups of subcomplexes in TNBC cells, which would allow for greater specificity in the definition of "PRC2-independent" non-canonical activity.

Finally, we utilize migration and tumorsphere assays to demonstrate cancer-relevant phenotypic impacts of EZH2-NF-κB signaling in TNBC cells. In all, we found non-canonical, PRC2-independent EZH2 activity to be the most important for maintaining or promoting malignant phenotypes, suggesting that the current therapeutic strategies targeting only canonical EZH2 catalytic activity or PRC2 interactions may be incompletely effective. EZH2 inhibition may display anti-tumor effects both in models and clinical trials, however, as epidrugs as monotherapy are already known to face primary resistance in solid tumors and non-canonical EZH2 activity independently drives oncogenic phenotypes, we believe identifying non-canonical EZH2 targets for combination therapeutic strategies would improve efficacy. From our analyses, we can derive non-canonical EZH2 targets for *in vitro* and *in vivo* validation considering not only EZH2 and NF-κB themselves, but also co-activated genes such as *CYR61/CCN1*. *In vivo* assessment of whether targeting both canonical and non-canonical EZH2 is more efficacious over targeting either individually would be critical to determine clinical value.

The data reported here support and expand upon prior reports of non-canonical EZH2 activation of NF-κB in TNBC cells; we provide a genomic profile and define target genes of EZH2 and NF-κB, link an EZH2 structural domain with NF-κB functional cooperation, and demonstrate both the impact of this pathway on oncogenic phenotypes and enrichment in TNBC/BLBC patient samples.

Limitations of the study

While our presented findings support PRC2-independent EZH2 co-activation of a subset of NF-κB target genes contributing to malignant phenotypes of TNBC cells, there are a few limitations to the study. While we suggest non-canonical EZH2 gene activation may present challenges to clinical applications

of EZH2 inhibitors as monotherapy, as indidvidual inhibitors have exhibited disappointing clinical results, this is ultimately speculation based on our proposed model. Catalytic EZH2 activity is demonstrably important for malignant phenotypes, but directly evaluating the individual contributions of non-canonical EZH2 is technically difficult given the lack of molecules that specifically target non-canonical activities, and as non-canonical activities vary in a context-dependent manner. Thus, as in our study, differences between total EZH2 targeting and canonical-only EZH2 targeting are considered to infer the importance of non-canonical EZH2. Additionally, while we observe changes in malignant phenotypes *in vitro* to demonstrate the importance of the EZH2 TAD and canonical vs. total EZH2, we do not evaluate these contributions *in vivo*. Based on previously published reports with MS177, we expect treatment with MS177 would result in reduced xenograft growth, or similar results in related *in vivo* applications. Similarly, we expect mutant TAD EZH2 (i.e. canonical-only) may be less malignant than WT EZH2 when assessed *in vivo*, but these applications are time-consuming and costly to undertake, and ultimately do not isolate non-canonical EZH2 or EZH2-NF-κB co-activation for evaluation in TNBC malignancy.

STAR★METHODS

Detailed methods are provided in the online version of this paper and include the following:

- KEY RESOURCES TABLE
- RESOURCE AVAILABILITY
  - Lead contact
  - Materials availability
  - Data and code availability
- EXPERIMENTAL MODEL AND STUDY PARTICIPANT DETAILS
  - Cell lines
- METHOD DETAILS
  - Transfection and generation of cell lines
  - Reverse transcription quantitative PCR
  - Immunoblotting and signal quantification
  - Chromatin immunoprecipitation (ChIP) qPCR
  - ChIP-seq
  - RNA-seq
  - Gene set enrichment analysis
  - Luciferase reporter assay
  - Immunoprecipitation and HA-IP
  - GST fusion recombinant protein pulldown
  - Migration assay
  - Tumorsphere assay
  - Soft agar colony formation assay
- QUANTIFICATION AND STATISTICAL ANALYSIS

SUPPLEMENTAL INFORMATION

Supplemental information can be found online at https://doi.org/10.1016/j.isci.2023.107115.

ACKNOWLEDGMENTS

We thank the members of the Baldwin and Wang laboratories for their useful insights and support in the conceptualization and reporting of this work. We thank the laboratory of Dr. Lindsey James for their generous provision of materials. We thank the High Throughput Sequencing Facility at UNC Chapel Hill for their expertize and sequencing services. This work was supported by NIH grants F31CA250362 (GJD), R01CA218600 (GGW), R01CA268519 (GGW), and R35CA197684 (ASB).

AUTHOR CONTRIBUTIONS

Conceptualization, G.J.D. and A.S.B.; Methodology, G.J.D. and J.W.; Investigation: G.J.D. and J.W.; Formal analysis, J.M.S. and G.J.D.; Data curation, J.M.S.; Resources, G.G.W. and A.S.B.; Visualization, G.J.D.; Writing—Original Draft, G.J.D.; Writing—Review & Editing, G.J.D., J.W., J.M.S., G.G.W., and A.S.B.; Supervision, A.S.B.; Funding Acquisition, G.J.D., G.G.W., and A.S.B.

DECLARATION OF INTERESTS

The authors declare no competing interests.

Received: March 8, 2023
Revised: May 10, 2023
Accepted: June 9, 2023
Published: June 14, 2023

REFERENCES

1. Cao, R., Wang, L., Wang, H., Xia, L., Erdjument-Bromage, H., Tempst, P., Jones, R.S., and Zhang, Y. (2002). Role of histone H3 lysine 27 methylation in Polycomb-group silencing. Science *298*, 1039–1043. https://doi.org/10.1126/SCIENCE.1076997.

2. Cao, R., and Zhang, Y. (2004). SUZ12 is required for both the histone methyltransferase activity and the silencing function of the EED-EZH2 complex. Mol. Cell. *15*, 57–67. https://doi.org/10.1016/j.molcel.2004.06.020.

3. Margueron, R., and Reinberg, D. (2011). The Polycomb complex PRC2 and its mark in life. Nature *469*, 343–349. https://doi.org/10.1038/nature09784.

4. Laugesen, A., Højfeldt, J.W., and Helin, K. (2019). Molecular Mechanisms Directing PRC2 Recruitment and H3K27 Methylation. Mol. Cell. *74*, 8–18. https://doi.org/10.1016/j.molcel.2019.03.011.

5. O'Carroll, D., Erhardt, S., Pagani, M., Barton, S.C., Surani, M.A., and Jenuwein, T. (2001). The Polycomb-Group Gene Ezh2 Is Required for Early Mouse Development. Mol. Cell Biol. *21*, 4330–4336. https://doi.org/10.1128/MCB.21.13.4330-4336.2001.

6. Ezhkova, E., Pasolli, H.A., Parker, J.S., Stokes, N., Su, I.H., Hannon, G., Tarakhovsky, A., and Fuchs, E. (2009). Ezh2 Orchestrates Gene Expression for the Stepwise Differentiation of Tissue-Specific Stem Cells. Cell *136*, 1122–1135. https://doi.org/10.1016/j.cell.2008.12.043.

7. Varambally, S., Dhanasekaran, S.M., Zhou, M., Barrette, T.R., Kumar-Sinha, C., Sanda, M.G., Ghosh, D., Pienta, K.J., Sewalt, R.G.A.B., Otte, A.P., et al. (2002). The polycomb group protein EZH2 is involved in progression of prostate cancer. Nature *419*, 624–629. https://doi.org/10.1038/nature01075.

8. Kleer, C.G., Cao, Q., Varambally, S., Shen, R., Ota, I., Tomlins, S.A., Ghosh, D., Sewalt, R.G.A.B., Otte, A.P., Hayes, D.F., et al. (2003). EZH2 is a marker of aggressive breast cancer and promotes neoplastic transformation of breast epithelial cells. Proc. Natl. Acad. Sci. USA *100*, 11606–11611. https://doi.org/10.1073/pnas.1933744100.

9. Bachmann, I.M., Halvorsen, O.J., Collett, K., Stefansson, I.M., Straume, O., Haukaas, S.A., Salvesen, H.B., Otte, A.P., and Akslen, L.A. (2006). EZH2 expression is associated with high proliferation rate and aggressive tumor subgroups in cutaneous melanoma and cancers of the endometrium, prostate, and breast. J. Clin. Oncol. *24*, 268–273. https://doi.org/10.1200/JCO.2005.01.5180.

10. Cao, Q., Yu, J., Dhanasekaran, S.M., Kim, J.H., Mani, R.S., Tomlins, S.A., Mehra, R., Laxman, B., Cao, X., Yu, J., et al. (2008). Repression of E-cadherin by the polycomb group protein EZH2 in cancer. Oncogene *27*, 7274–7284. https://doi.org/10.1038/onc.2008.333.

11. Zong, X., Wang, W., Ozes, A., Fang, F., Sandusky, G.E., and Nephew, K.P. (2020). EZH2-mediated Downregulation of the Tumor Suppressor DAB2IP Maintains Ovarian Cancer Stem Cells. Cancer Res. *80*, 4371–4385. https://doi.org/10.1158/0008-5472.can-20-0458.

12. Wang, X., Hu, B., Shen, H., Zhou, H., Xue, X., Chen, Y., Chen, S., Han, Y., Yuan, B., Zhao, H., et al. (2015). Clinical and prognostic relevance of EZH2 in breast cancer: A meta-analysis. Biomed. Pharmacother. *75*, 218–225. https://doi.org/10.1016/J.BIOPHA.2015.07.038.

13. Souroullas, G.P., Jeck, W.R., Parker, J.S., Simon, J.M., Liu, J.Y., Paulk, J., Xiong, J., Clark, K.S., Fedoriw, Y., Qi, J., et al. (2016). An oncogenic Ezh2 mutation induces tumors through global redistribution of histone 3 lysine 27 trimethylation. Nat. Med. *22*, 632–640. https://doi.org/10.1038/nm.4092.

14. Chase, A., and Cross, N.C.P. (2011). Aberrations of EZH2 in cancer. Clin. Cancer Res. *17*, 2613–2618. https://doi.org/10.1158/1078-0432.CCR-10-2156.

15. Kim, K.H., and Roberts, C.W.M. (2016). Targeting EZH2 in cancer. Nat. Med. *22*, 128–134. https://doi.org/10.1038/nm.4036.

16. Bhat, K.P., Ümit Kaniskan, H., Jin, J., and Gozani, O. (2021). Epigenetics and beyond: targeting writers of protein lysine methylation to treat disease. Nat. Rev. Drug Discov. *20*, 265–286. https://doi.org/10.1038/s41573-020-00108-x.

17. McCabe, M.T., Ott, H.M., Ganji, G., Korenchuk, S., Thompson, C., van Aller, G.S., Liu, Y., Graves, A.P., Della Pietra, A., 3rd, Diaz, E., et al. (2012). EZH2 inhibition as a therapeutic strategy for lymphoma with EZH2-activating mutations. Nature *492*, 108–112. https://doi.org/10.1038/nature11606.

18. Yang, X., Li, F., Konze, K.D., Meslamani, J., Ma, A., Brown, P.J., Zhou, M.M., Arrowsmith, C.H., Kaniskan, H.Ü., Vedadi, M., and Jin, J. (2016). Structure-activity relationship studies for enhancer of zeste homologue 2 (EZH2) and enhancer of zeste homologue 1 (EZH1) inhibitors. J. Med. Chem. *59*, 7617–7633. https://doi.org/10.1021/acs.jmedchem.6b00855.

19. Zhao, Y., Guan, Y.Y., Zhao, F., Yu, T., Zhang, S.J., Zhang, Y.Z., Duan, Y.C., and Zhou, X.L. (2022). Recent strategies targeting Embryonic Ectoderm Development (EED) for cancer therapy: Allosteric inhibitors, PPI inhibitors, and PROTACs. Eur. J. Med. Chem. *231*, 114144. https://doi.org/10.1016/J.EJMECH.2022.114144.

20. Richart, L., and Margueron, R. (2020). Drugging histone methyltransferases in cancer. Curr. Opin. Chem. Biol. *56*, 51–62. https://doi.org/10.1016/j.cbpa.2019.11.009.

21. He, Y., Selvaraju, S., Curtin, M.L., Jakob, C.G., Zhu, H., Comess, K.M., Shaw, B., The, J., Lima-Fernandes, E., Szewczyk, M.M., et al. (2017). The EED protein-protein interaction inhibitor A-395 inactivates the PRC2 complex. Nat. Chem. Biol. *13*, 389–395. https://doi.org/10.1038/nchembio.2306.

22. Potjewyd, F., Turner, A.M.W., Beri, J., Rectenwald, J.M., Norris-Drouin, J.L., Cholensky, S.H., Margolis, D.M., Pearce, K.H., Herring, L.E., and James, L.I. (2020). Degradation of Polycomb Repressive Complex 2 with an EED-Targeted Bivalent Chemical Degrader. Cell Chem. Biol. *27*, 47–56.e15. https://doi.org/10.1016/j.chembiol.2019.11.006.

23. Italiano, A., Soria, J.C., Toulmonde, M., Michot, J.M., Lucchesi, C., Varga, A., Coindre, J.M., Blakemore, S.J., Clawson, A., Suttle, B., et al. (2018). Tazemetostat, an EZH2 inhibitor, in relapsed or refractory B-cell non-Hodgkin lymphoma and advanced solid tumours: a first-in-human, open-label, phase 1 study. Lancet Oncol. *19*, 649–659. https://doi.org/10.1016/S1470-2045(18)30145-1.

24. Garapaty-Rao, S., Nasveschuk, C., Gagnon, A., Chan, E.Y., Sandy, P., Busby, J., Balasubramanian, S., Campbell, R., Zhao, F., Bergeron, L., et al. (2013). Identification of EZH2 and EZH1 Small Molecule Inhibitors with Selective Impact on Diffuse Large B Cell Lymphoma Cell Growth. Chem. Biol. (Lond.) *20*, 1329–1339. https://doi.org/10.1016/J.CHEMBIOL.2013.09.013.

25. Xu, B., On, D.M., Ma, A., Parton, T., Konze, K.D., Pattenden, S.G., Allison, D.F., Cai, L., Rockowitz, S., Liu, S., et al. (2015). Selective inhibition of EZH2 and EZH1 enzymatic

activity by a small molecule suppresses MLL-rearranged leukemia. Blood *125*, 346–357. https://doi.org/10.1182/blood-2014-06-581082.

26. Yap, T.A., Winter, J.N., Giulino-Roth, L., Longley, J., Lopez, J., Michot, J.M., Leonard, J.P., Ribrag, V., McCabe, M.T., Creasy, C.L., et al. (2019). Phase I study of the novel enhancer of zeste homolog 2 (EZH2) inhibitor GSK2816126 in patients with advanced hematologic and solid tumors. Clin. Cancer Res. *25*, 7331–7339. https://doi.org/10.1158/1078-0432.CCR-18-4121.

27. Wang, J., and Wang, G.G. (2020). No easy way out for ezh2: Its pleiotropic, noncanonical effects on gene regulation and cellular function. Int. J. Mol. Sci. *21*, 9501–9516. https://doi.org/10.3390/ijms21249501.

28. Xu, K., Wu, Z.J., Groner, A.C., He, H.H., Cai, C., Lis, R.T., Wu, X., Stack, E.C., Loda, M., Liu, T., et al. (2012). EZH2 Oncogenic Activity in Castration-Resistant Prostate Cancer Cells Is Polycomb-Independent. Science *338*, 1465–1469. https://doi.org/10.1126/science.1227604.

29. Kim, J., Lee, Y., Lu, X., Song, B., Fong, K.W., Cao, Q., Licht, J.D., Zhao, J.C., and Yu, J. (2018). Polycomb- and Methylation-Independent Roles of EZH2 as a Transcription Activator. Cell Rep. *25*, 2808–2820.e4. https://doi.org/10.1016/j.celrep.2018.11.035.

30. Lee, S.T., Li, Z., Wu, Z., Aau, M., Guan, P., Karuturi, R.K.M., Liou, Y.C., and Yu, Q. (2011). Context-Specific Regulation of NF-κB Target Gene Expression by EZH2 in Breast Cancers. Mol. Cell. *43*, 798–810. https://doi.org/10.1016/j.molcel.2011.08.011.

31. Wang, J., Yu, X., Gong, W., Liu, X., Park, K.S., Ma, A., Tsai, Y.H., Shen, Y., Onikubo, T., Pi, W.C., et al. (2022). EZH2 noncanonically binds cMyc and p300 through a cryptic transactivation domain to mediate gene activation and promote oncogenesis. Nat. Cell Biol. *24*, 384–399. https://doi.org/10.1038/s41556-022-00850-x.

32. Davies, A., Nouruzi, S., Ganguli, D., Namekawa, T., Thaper, D., Linder, S., Karaoğlanoğlu, F., Omur, M.E., Kim, S., Kobelev, M., et al. (2021). An androgen receptor switch underlies lineage infidelity in treatment-resistant prostate cancer. Nat. Cell Biol. *23*, 1023–1034. https://doi.org/10.1038/s41556-021-00743-5.

33. Kim, E., Kim, M., Woo, D.H., Shin, Y., Shin, J., Chang, N., Oh, Y.T., Kim, H., Rheey, J., Nakano, I., et al. (2013). Phosphorylation of EZH2 Activates STAT3 Signaling via STAT3 Methylation and Promotes Tumorigenicity of Glioblastoma Stem-like Cells. Cancer Cell *23*, 839–852. https://doi.org/10.1016/j.ccr.2013.04.008.

34. Pereira, B., Chin, S.-F., Rueda, O.M., Vollan, H.-K.M., Provenzano, E., Bardwell, H.A., Pugh, M., Jones, L., Russell, R., Sammut, S.-J., et al. (2016). The somatic mutation profiles of 2,433 breast cancers refine their genomic and transcriptomic landscapes. Nat. Commun. *7*, 11479. https://doi.org/10.1038/ncomms11479.

35. Yomtoubian, S., Lee, S.B., Verma, A., Izzo, F., Markowitz, G., Choi, H., Cerchietti, L., Vahdat, L., Brown, K.A., Andreopoulou, E., et al. (2020). Inhibition of EZH2 Catalytic Activity Selectively Targets a Metastatic Subpopulation in Triple-Negative Breast Cancer. Cell Rep. *30*, 755–770.e6. https://doi.org/10.1016/j.celrep.2019.12.056.

36. Rueda, O.M., Sammut, S.J., Seoane, J.A., Chin, S.F., Caswell-Jin, J.L., Callari, M., Batra, R., Pereira, B., Bruna, A., Ali, H.R., et al. (2019). Dynamics of breast-cancer relapse reveal late-recurring ER-positive genomic subgroups. Nature *567*, 399–404. https://doi.org/10.1038/S41586-019-1007-8.

37. Curtis, C., Shah, S.P., Chin, S.F., Turashvili, G., Rueda, O.M., Dunning, M.J., Speed, D., Lynch, A.G., Samarajiwa, S., Yuan, Y., et al. (2012). The genomic and transcriptomic architecture of 2,000 breast tumours reveals novel subgroups. Nature *486*, 346–352. https://doi.org/10.1038/NATURE10983.

38. Yang, C.-C., LaBaff, A., Wei, Y., Nie, L., Xia, W., Huo, L., Yamaguchi, H., Hsu, Y.-H., Hsu, J.L., Liu, D., et al. (2015). Phosphorylation of EZH2 at T416 by CDK2 contributes to the malignancy of triple negative breast cancers. Am. J. Transl. Res. *7*, 1009–1020.

39. Nie, L., Wei, Y., Zhang, F., Hsu, Y.-H., Chan, L.-C., Xia, W., Ke, B., Zhu, C., Deng, R., Tang, J., et al. (2019). CDK2-mediated site-specific phosphorylation of EZH2 drives and maintains triple-negative breast cancer. Nat. Commun. *10*, 5114. https://doi.org/10.1038/s41467-019-13105-5.

40. Yin, L., Duan, J.J., Bian, X.W., and Yu, S.C. (2020). Triple-negative breast cancer molecular subtyping and treatment progress. Breast Cancer Res. *22*, 61. https://doi.org/10.1186/S13058-020-01296-5.

41. Pires, B.R.B., Mencalha, A.L., Ferreira, G.M., De Souza, W.F., Morgado-Díaz, J.A., Maia, A.M., Corrêa, S., and Abdelhay, E.S.F.W. (2017). NF-kappaB is involved in the regulation of EMT genes in breast cancer cells. PLoS One *12*, 01696222–e169720. https://doi.org/10.1371/journal.pone.0169622.

42. Yamaguchi, N., Ito, T., Azuma, S., Ito, E., Honma, R., Yanagisawa, Y., Nishikawa, A., Kawamura, M., Imai, J.i., Watanabe, S., et al. (2009). Constitutive activation of nuclear factor-κB is preferentially involved in the proliferation of basal-like subtype breast cancer cell lines. Cancer Sci. *100*, 1668–1674. https://doi.org/10.1111/j.1349-7006.2009.01228.x.

43. Hoesel, B., and Schmid, J.A. (2013). The complexity of NF- κB signaling in inflammation and cancer. Mol. Cancer *12*, 86. https://doi.org/10.1186/1476-4598-12-86.

44. Kendellen, M.F., Bradford, J.W., Lawrence, C.L., Clark, K.S., and Baldwin, A.S. (2014). Canonical and non-canonical NF-κB signaling promotes breast cancer tumor-initiating cells. Oncogene *33*, 1297–1305. https://doi.org/10.1038/onc.2013.64.

45. Hartman, Z.C., Poage, G.M., Den Hollander, P., Tsimelzon, A., Hill, J., Panupinthu, N., Zhang, Y., Mazumdar, A., Hilsenbeck, S.G., Mills, G.B., and Brown, P.H. (2013). Growth of triple-negative breast cancer cells relies upon coordinate autocrine expression of the proinflammatory cytokines IL-6 and IL-8. Cancer Res. *73*, 3470–3480. https://doi.org/10.1158/0008-5472.CAN-12-4524-T.

46. Taniguchi, K., and Karin, M. (2018). NF-κB, inflammation, immunity and cancer: coming of age. Nat. Rev. Immunol. *18*, 309–324. https://doi.org/10.1038/nri.2017.142.

47. Bianchini, G., Balko, J.M., Mayer, I.A., Sanders, M.E., and Gianni, L. (2016). Triple-negative breast cancer: Challenges and opportunities of a heterogeneous disease. Nat. Rev. Clin. Oncol. *13*, 674–690. https://doi.org/10.1038/nrclinonc.2016.66.

48. Lee, A., and Djamgoz, M.B.A. (2018). Triple negative breast cancer: Emerging therapeutic modalities and novel combination therapies. Cancer Treat Rev. *62*, 110–122. https://doi.org/10.1016/j.ctrv.2017.11.003.

49. Wang, X., Belguise, K., Kersual, N., Kirsch, K.H., Mineva, N.D., Galtier, F., Chalbos, D., and Sonenshein, G.E. (2007). Oestrogen signalling inhibits invasive phenotype by repressing RelB and its target BCL2. Nat. Cell Biol. *9*, 470–478. https://doi.org/10.1038/ncb1559.

50. Wang, X., Fang, Y., Sun, W., Xu, Z., Zhang, Y., Wei, X., Ding, X., and Xu, Y. (2020). Endocrinotherapy resistance of prostate and breast cancer: Importance of the NF–κB pathway (Review). Int. J. Oncol. *56*, 1064–1074. https://doi.org/10.3892/ijo.2020.4990.

51. Lawrence, C.L., and Baldwin, A.S. (2016). Non-Canonical EZH2 Transcriptionally Activates RelB in Triple Negative Breast Cancer. PLoS One *11*, e0165005. https://doi.org/10.1371/journal.pone.0165005.

52. Jiao, L., Shubbar, M., Yang, X., Zhang, Q., Chen, S., Wu, Q., and Chen, Z. (2020). A Partially Disordered Region Connects Gene Repression and Activation Functions of EZH2. 1–11. https://doi.org/10.1073/pnas.1914866117.

53. Wang, J., Park, K.-S., Yu, X., Gong, W., Earp, H.S., Wang, G.G., Jin, J., and Cai, L. (2022). A cryptic transactivation domain of EZH2 binds AR and AR's splice variant, promoting oncogene activation and tumorous transformation. Nucleic Acids Res. *50*, 10929–10946. https://doi.org/10.1093/nar/gkac861.

54. Espinoza, I., Kurapaty, C., Park, C.-H., vander Steen, T., Kleer, C.G., Wiley, E., Rademaker, A., Cuyàs, E., Verdura, S., Buxó, M., et al. (2022). Depletion of CCN1/CYR61 reduces triple-negative/basal-like breast cancer aggressiveness. Am. J. Cancer Res. *12*, 839–851.

55. Tsai, M.-S., Bogart, D.F., Castañeda, J.M., Li, P., and Lupu, R. (2002). Cyr61 promotes

breast tumorigenesis and cancer progression. Oncogene *21*, 8178–8185. https://doi.org/10.1038/sj.onc.1205682.

56. Mayer, S., Erbes, T., Timme-Bronsert, S., Jaeger, M., Rücker, G., Kuf, F., Stickeler, E., Gitsch, G., and Hirschfeld, M. (2017). Clinical relevance of cyr61 expression in patients with hormone-dependent breast cancer. Oncol. Lett. *14*, 2334–2340. https://doi.org/10.3892/ol.2017.6406.

57. Chen, H., Tu, S.W., and Hsieh, J.T. (2005). Down-regulation of human DAB2IP gene expression mediated by polycomb Ezh2 complex and histone deacetylase in prostate cancer. J. Biol. Chem. *280*, 22437–22444. https://doi.org/10.1074/jbc.M501379200.

58. Kirmizis, A., Bartley, S.M., Kuzmichev, A., Margueron, R., Reinberg, D., Green, R., and Farnham, P.J. (2004). Silencing of human polycomb target genes is associated with methylation of histone H3 Lys 27. Genes Dev. *18*, 1592–1605. https://doi.org/10.1101/GAD.1200204.

59. Messier, T.L., Boyd, J.R., Gordon, J.A.R., Stein, J.L., Lian, J.B., and Stein, G.S. (2016). Oncofetal Epigenetic Bivalency in Breast Cancer Cells: H3K4 and H3K27 Tri-Methylation as a Biomarker for Phenotypic Plasticity. J. Cell. Physiol. *231*, 2474–2481. https://doi.org/10.1002/jcp.25359.

60. Tanaka, H., Takizawa, Y., Takaku, M., Kato, D., Kumagawa, Y., Grimm, S.A., Wade, P.A., and Kurumizaka, H. (2020). Interaction of the pioneer transcription factor GATA3 with nucleosomes. Nat. Commun. *11*, 4136. https://doi.org/10.1038/s41467-020-17959-y.

61. Takaku, M., Grimm, S.A., Shimbo, T., Perera, L., Menafra, R., Stunnenberg, H.G., Archer, T.K., Machida, S., Kurumizaka, H., and Wade, P.A. (2016). GATA3-dependent cellular reprogramming requires activation-domain dependent recruitment of a chromatin remodeler. Genome Biol. *17*, 36. https://doi.org/10.1186/s13059-016-0897-0.

62. Zabel, U., Schreck, R., and Baeuerle, P.A. (1991). DNA binding of purified transcription factor NF-kappa B. Affinity, specificity, Zn2+ dependence, and differential half-site recognition. J. Biol. Chem. *266*, 252–260. https://doi.org/10.1016/S0021-9258(18)52428-5.

63. Kawakami, K., Scheidereit, C., and Roeder, R.G. (1988). Identification and purification of a human immunoglobulin-enhancer-binding protein (NF-kappa B) that activates transcription from a human immunodeficiency virus type 1 promoter in vitro. Proc. Natl. Acad. Sci. USA *85*, 4700–4704. https://doi.org/10.1073/PNAS.85.13.4700.

64. Heinz, S., Benner, C., Spann, N., Bertolino, E., Lin, Y.C., Laslo, P., Cheng, J.X., Murre, C., Singh, H., and Glass, C.K. (2010). Simple Combinations of Lineage-Determining Transcription Factors Prime cis-Regulatory Elements Required for Macrophage and B Cell Identities. Mol. Cell. *38*, 576–589. https://doi.org/10.1016/J.MOLCEL.2010.05.004.

65. Bren, G.D., Solan, N.J., Miyoshi, H., Pennington, K.N., Pobst, L.J., and Paya, C.v. (2001). Transcription of the RelB gene is regulated by NF-κB. Oncogene *20*, 7722–7733. https://doi.org/10.1038/sj.onc.1204868.

66. Solan, N.J., Miyoshi, H., Carmona, E.M., Bren, G.D., and Paya, C.v. (2002). RelB cellular regulation and transcriptional activity are regulated by p100. J. Biol. Chem. *277*, 1405–1418. https://doi.org/10.1074/jbc.M109619200.

67. Oeckinghaus, A., and Ghosh, S. (2009). The NF- B Family of Transcription Factors and Its Regulation. Cold Spring Harbor Perspect. Biol. *1*, a000034. https://doi.org/10.1101/cshperspect.a000034.

68. Forozan, F., Veldman, R., Ammerman, C.A., Parsa, N.Z., Kallioniemi, A., Kallioniemi, O.P., and Ethier, S.P. (1999). Molecular cytogenetic analysis of 11 new breast cancer cell lines. Br. J. Cancer *81*, 1328–1334. https://doi.org/10.1038/SJ.BJC.6695007.

69. van Golen, K.L., Davies, S., Wu, Z.F., Wang, Y., Bucana, C.D., Root, H., Chandrasekharappa, S., Strawderman, M., Ethier, S.P., and Merajver, S.D. (1999). A Novel Putative Low-Affinity Insulin-like Growth Factor-binding Protein, LIBC (Lost in Inflammatory Breast Cancer), and RhoC GTPase Correlate with the Inflammatory Breast Cancer Phenotype. Clin. Cancer Res. *5*, 2511–2519. https://aacrjournals.org/clincancerres/article/5/9/2511/287842/A-Novel-Putative-Low-Affinity-Insulin-like-Growth.

70. Ngo, K.A., Kishimoto, K., Davis-Turak, J., Pimplaskar, A., Cheng, Z., Spreafico, R., Chen, E.Y., Tam, A., Ghosh, G., Mitchell, S., and Hoffmann, A. (2020). Dissecting the Regulatory Strategies of NF-κB RelA Target Genes in the Inflammatory Response Reveals Differential Transactivation Logics. Cell Rep. *30*, 2758–2775.e6. https://doi.org/10.1016/j.celrep.2020.01.108.

71. Smale, S.T. (2012). Dimer-specific regulatory mechanisms within the NF-κB family of transcription factors. Immunol. Rev. *246*, 193–204. https://doi.org/10.1111/j.1600-065X.2011.01091.x.

72. Choe, U., Yu, L., and Wang, T.T.Y. (2019). Selected lipid-based transfection reagents activate NF-κB and MAP kinases signaling pathways, induced cytokines mRNA expression in human THP-1 macrophage. Anal. Biochem. *573*, 73–76. https://doi.org/10.1016/J.AB.2019.02.018.

73. Margueron, R., Justin, N., Ohno, K., Sharpe, M.L., Son, J., Drury, W.J., III, Voigt, P., Martin, S.R., Taylor, W.R., De Marco, V., et al. (2009). Role of the polycomb protein EED in the propagation of repressive histone marks. Nature *461*, 762–767. https://doi.org/10.1038/nature08398.

74. Onyeisi, J.O.S., Greve, B., Espinoza-Sánchez, N.A., Kiesel, L., Lopes, C.C., and Götte, M. (2021). microRNA-140-3p modulates invasiveness, motility, and extracellular matrix adhesion of breast cancer cells by targeting syndecan-4. J. Cell. Biochem. *122*, 1491–1505. https://doi.org/10.1002/JCB.30071.

75. Onyeisi, J.O.S., Lopes, C.C., and Götte, M. (2022). Role of syndecan-4 in breast cancer pathophysiology. Am. J. Physiol. Cell Physiol. *323*, C1345–C1354. https://doi.org/10.1152/ajpcell.00152.2022.

76. Liao, W.-C., Yen, H.-R., Chen, C.-H., Chu, Y.-H., Song, Y.-C., Tseng, T.-J., and Liu, C.-H. (2021). CHPF promotes malignancy of breast cancer cells by modifying syndecan-4 and the tumor microenvironment. Am. J. Cancer Res. *11*, 812–826.

77. Kwon, A., Lee, H.L., Woo, K.M., Ryoo, H.M., and Baek, J.H. (2013). SMURF1 plays a role in EGF-induced breast cancer cell migration and invasion. Mol. Cell. *36*, 548–555. https://doi.org/10.1007/S10059-013-0233-4.

78. Kawabata, H., Azuma, K., Ikeda, K., Sugitani, I., Kinowaki, K., Fujii, T., Osaki, A., Saeki, T., Horie-Inoue, K., and Inoue, S. (2017). TRIM44 Is a Poor Prognostic Factor for Breast Cancer Patients as a Modulator of NF-κB Signaling. Int. J. Mol. Sci. *18*, 1931. https://doi.org/10.3390/IJMS18091931.

79. Baldwin, A.S., Azizkhan, J.C., Jensen, D.E., Beg, A.A., and Coodly, L.R. (1991). Induction of NF-kappa B DNA-binding activity during the G0-to-G1 transition in mouse fibroblasts. Mol. Cell Biol. *11*, 4943–4951. https://doi.org/10.1128/mcb.11.10.4943-4951.1991.

80. Prat, A., Parker, J.S., Karginova, O., Fan, C., Livasy, C., Herschkowitz, J.I., He, X., and Perou, C.M. (2010). Phenotypic and molecular characterization of the claudin-low intrinsic subtype of breast cancer. Breast Cancer Res. *12*, R68. https://doi.org/10.1186/bcr2635.

81. Perou, C.M., Sørlie, T., Eisen, M.B., van de Rijn, M., Jeffrey, S.S., Rees, C.A., Pollack, J.R., Ross, D.T., Johnsen, H., Akslen, L.A., et al. (2000). Molecular portraits of human breast tumours. Nature *406*, 747–752. https://doi.org/10.1038/35021093.

82. Cancer Genome Atlas Network, Fulton, R.S., McLellan, M.D., Schmidt, H., Kalicki-Veizer, J., McMichael, J.F., Fulton, L.L., Dooling, D.J., Ding, L., Mardis, E.R., et al. (2012). Comprehensive molecular portraits of human breast tumours. Nature *490*, 61–70. https://doi.org/10.1038/nature11412.

83. Liu, W., Wen, Y., Wang, M., Gui, S., Li, X., Fan, Y., Yan, X., Lin, Y., Sun, Y., Liu, J., et al. (2018). An Integrated TCGA Pan-Cancer Clinical Data Resource to Drive High-Quality Survival Outcome Analytics. Cell *18*, 400–408. https://doi.org/10.1016/j.cell.2018.02.052.

84. Gao, J., Aksoy, B.A., Dogrusoz, U., Dresdner, G., Gross, B., Sumer, S.O., Sun, Y., Jacobsen, A., Sinha, R., Larsson, E., et al. (2013). Integrative Analysis of Complex Cancer Genomics and Clinical Profiles Using the cBioPortal. Sci. Signal. *6*, 1. https://doi.org/10.1126/scisignal.2004088.

85. Cerami, E., Gao, J., Dogrusoz, U., Gross, B.E., Sumer, S.O., Aksoy, B.A., Jacobsen, A., Byrne, C.J., Heuer, M.L., Larsson, E., et al. (2012). The cBio Cancer Genomics Portal: An open platform for exploring multidimensional cancer genomics data. Cancer Discov. *2*, 401–404. https://doi.org/10.1158/2159-8290.CD-12-0095.

86. Krug, K., Jaehnig, E.J., Satpathy, S., Blumenberg, L., Karpova, A., Anurag, M., Miles, G., Mertins, P., Geffen, Y., Tang, L.C., et al. (2020). Proteogenomic Landscape of Breast Cancer Tumorigenesis and Targeted Therapy. Cell *183*, 1436–1456.e31. https://doi.org/10.1016/j.cell.2020.10.036.

87. ICGC/TCGA Pan-Cancer Analysis of Whole Genomes Consortium, Abascal, F., Abeshouse, A., Aburatani, H., Adams, D.J., Agrawal, N., Ahn, K.S., Ahn, S.-M., Aikata, H., Akbani, R., et al. (2020). Pan-cancer analysis of whole genomes. Nature *578*, 82–93. https://doi.org/10.1038/s41586-020-1969-6.

88. Sun, S.-C. (2011). Non-canonical NF-κB signaling pathway. Cell Res. *21*, 71–85. https://doi.org/10.1038/cr.2010.177.

89. Marienfeld, R., May, M.J., Berberich, I., Serfling, E., Ghosh, S., and Neumann, M. (2003). RelB forms transcriptionally inactive complexes with RelA/p65. J. Biol. Chem. *278*, 19852–19860. https://doi.org/10.1074/jbc.M301945200.

90. Jacque, E., Tchenio, T., Piton, G., Romeo, P.-H., and Ronique Baud, V. (2005). RelA repression of RelB activity induces selective gene activation downstream of TNF receptors. Proc. Natl. Acad. Sci. USA *102*, 14635–14640. https://doi.org/10.1073/pnas.0507342102.

91. Mitchell, S., Vargas, J., and Hoffmann, A. (2016). Signaling via the NFκB system. Wiley Interdiscip. Rev. Syst. Biol. Med. *8*, 227–241. https://doi.org/10.1002/wsbm.1331.

92. Cha, T.-L., Zhou, B.P., Xia, W., Wu, Y., Yang, C.-C., Chen, C.-T., Ping, B., Otte, A.P., and Hung, M.-C. (2005). Akt-mediated phosphorylation of EZH2 suppresses methylation of lysine 27 in histone H3. Science *310*, 306–310. https://doi.org/10.1126/science.1118947.

93. Jiao, L., Shubbar, M., Yang, X., Zhang, Q., Chen, S., Wu, Q., Chen, Z., Rizo, J., and Liu, X. (2020). A partially disordered region connects gene repression and activation functions of EZH2. Proc. Natl. Acad. Sci. USA *117*, 16992–17002. https://doi.org/10.1073/pnas.1914866117.

94. Anwar, T., Gonzalez, M.E., and Kleer, C.G. (2021). Noncanonical Functions of the Polycomb Group Protein EZH2 in Breast Cancer. Am. J. Pathol. *191*, 774–783. https://doi.org/10.1016/j.ajpath.2021.01.013.

95. Xu, J., Shao, Z., Li, D., Xie, H., Kim, W., Huang, J., Taylor, J.E., Pinello, L., Glass, K., Jaffe, J.D., et al. (2015). Developmental control of polycomb subunit composition by GATA factors mediates a switch to non-canonical functions. Mol. Cell. *57*, 304–316. https://doi.org/10.1016/j.molcel.2014.12.009.

96. Martin, M. (2011). Cutadapt removes adapter sequences from high-throughput sequencing reads. EMBnet. j. *17*, 10. https://doi.org/10.14806/ej.17.1.200.

97. Dobin, A., Davis, C.A., Schlesinger, F., Drenkow, J., Zaleski, C., Jha, S., Batut, P., Chaisson, M., and Gingeras, T.R. (2013). STAR: ultrafast universal RNA-seq aligner. Bioinformatics *29*, 15–21. https://doi.org/10.1093/bioinformatics/bts635.

98. Zhang, Y., Liu, T., Meyer, C.A., Eeckhoute, J., Johnson, D.S., Bernstein, B.E., Nusbaum, C., Myers, R.M., Brown, M., Li, W., and Liu, X.S. (2008). Model-based Analysis of ChIP-Seq (MACS). Genome Biol. *9*, R137. https://doi.org/10.1186/gb-2008-9-9-r137.

99. Quinlan, A.R., and Hall, I.M. (2010). BEDTools: a flexible suite of utilities for comparing genomic features. Bioinformatics *26*, 841–842. https://doi.org/10.1093/bioinformatics/btq033.

100. Patro, R., Duggal, G., Love, M.I., Irizarry, R.A., and Kingsford, C. (2017). Salmon provides fast and bias-aware quantification of transcript expression. Nat. Methods *14*, 417–419. https://doi.org/10.1038/nmeth.4197.

101. Love, M.I., Huber, W., and Anders, S. (2014). Moderated estimation of fold change and dispersion for RNA-seq data with DESeq2. Genome Biol. *15*, 550. https://doi.org/10.1186/s13059-014-0550-8.

102. Kim, D., Paggi, J.M., Park, C., Bennett, C., and Salzberg, S.L. (2019). Graph-based genome alignment and genotyping with HISAT2 and HISAT-genotype. Nat. Biotechnol. *37*, 907–915. https://doi.org/10.1038/s41587-019-0201-4.

103. Liao, Y., Smyth, G.K., and Shi, W. (2014). featureCounts: an efficient general purpose program for assigning sequence reads to genomic features. Bioinformatics *30*, 923–930. https://doi.org/10.1093/bioinformatics/btt656.

104. Liberzon, A., Birger, C., Thorvaldsdóttir, H., Ghandi, M., Mesirov, J.P., and Tamayo, P. (2015). The Molecular Signatures Database Hallmark Gene Set Collection. Cell Syst. *1*, 417–425. https://doi.org/10.1016/j.cels.2015.12.004.

105. Ashburner, M., Ball, C.A., Blake, J.A., Botstein, D., Butler, H., Cherry, J.M., Davis, A.P., Dolinski, K., Dwight, S.S., Eppig, J.T., et al. (2000). Gene Ontology: tool for the unification of biology. Nat. Genet. *25*, 25–29. https://doi.org/10.1038/75556.

106. Gene Ontology Consortium, Douglass, E., Good, B.M., Unni, D.R., Harris, N.L., Mungall, C.J., Basu, S., Chisholm, R.L., Dodson, R.J., Hartline, E., et al. (2021). The Gene Ontology resource: enriching a GOld mine. Nucleic Acids Res. *49*, D325–D334. https://doi.org/10.1093/nar/gkaa1113.

107. Mi, H., Muruganujan, A., Casagrande, J.T., and Thomas, P.D. (2013). Large-scale gene function analysis with the PANTHER classification system. Nat. Protoc. *8*, 1551–1566. https://doi.org/10.1038/nprot.2013.092.

108. Subramanian, A., Tamayo, P., Mootha, V.K., Mukherjee, S., Ebert, B.L., Gillette, M.A., Paulovich, A., Pomeroy, S.L., Golub, T.R., Lander, E.S., and Mesirov, J.P. (2005). Gene set enrichment analysis: A knowledge-based approach for interpreting genome-wide expression profiles. Proc. Natl. Acad. Sci. USA *102*, 15545–15550. https://doi.org/10.1073/pnas.0506580102.

109. Jonkman, J.E.N., Cathcart, J.A., Xu, F., Bartolini, M.E., Amon, J.E., Stevens, K.M., and Colarusso, P. (2014). An introduction to the wound healing assay using live-cell microscopy. Cell Adhes. Migrat. *8*, 440–451. https://doi.org/10.4161/cam.36224.

STAR★METHODS

KEY RESOURCES TABLE

REAGENT or RESOURCE	SOURCE	IDENTIFIER
Antibodies		
Anti-Rabbit IgG HRP Conjugate	Promega	Cat# W4011; RRID:AB_430833
Anti-Mouse IgG HRP Conjugate	Promega	Cat# W4021; RRID:AB_430834
Donkey anti-sheep IgG HRP	LifeTech/Novex	Cat # A16041; RRID: AB_2534715
Clean-Blot IP Detection Reagent (HRP)	Thermo Fisher Scientific	Cat# 21230; RRID:AB_2864363
Beta-Actin Mouse mAb	Cell Signaling Technology	Cat# 3700; RRID: AB_2242334
GAPDH Rabbit mAb	Cell Signaling Technology	Cat# 5174; RRID: AB_ 10622025
EZH2 Rabbit mAb	Cell Signaling Technology	Cat# 5246; RRID: AB_10694683
RelA Rabbit mAb	Cell Signaling Technology	Cat# 8242; RRID:AB_10859369
RelB Rabbit mAb	Cell Signaling Technology	Cat# 4922; RRID:AB_2179173
NFKB2 p100/p52 Rabbit polyclonal	Cell Signaling Technology	Cat# 4882; RRID:AB_10695537
DAB2IP Rabbit polyclonal	Abcam	Cat# ab87811; RRID:AB_2041032
H3K27me3 Rabbit polyclonal	EMD Millipore	Cat# 07-449; RRID:AB_310624
H3K4me3 Rabbit mAb	Cell Signaling Technology	Cat# 9751; RRID:AB_2616028
HA Mouse mAb	Covance	Cat# MMS-101P; RRID:AB_2314672
SUZ12 Rabbit mAb	Cell Signaling Technology	Cat# 3737; RRID: AB_2196850
EED Sheep polyclonal	R&D Systems	Cat# AF5827; RRID: AB_2246350
Rabbit IgG Isotype Control	Cell Signaling Technology	Cat# 3900; RRID:AB_1550038
Bacterial and virus strains		
MAX Efficiency DH5alpha *E. coli*	Thermo Fisher Scientific	Cat# 18258012
One Shot Stbl3 *E. coli*	Thermo Fisher Scientific	Cat# C737303
Chemicals, peptides, and recombinant proteins		
TRIzol	Thermo Fisher Scientific	Cat# 15596026
DharmaFECT I Transfection Reagent	Dharmacon	Cat# T-2001-03
FuGene HD Transfection Reagent	Promega	Cat# E2311
Disuccinimidyl glutarate (DSG)	Thermo Fisher Scientific	Cat# A35392
16% Methanol Free Formaldehyde	Thermo Fisher Scientific	Cat# 28908
Protein G Dynabeads	Thermo Fisher Scientific	Cat# 10004D
Anti-HA conjugated magnetic beads	Thermo Fisher Scientific	Cat# 88836
Doxycycline hyclate	Sigma Aldrich	Cat# D9891
RNase A	Sigma Aldrich	Cat# 10109142001
Proteinase K	Sigma Aldrich	Cat# P2308
GSK126	Cayman Chemical Company	Cat# 15415
Tazemetostat	Selleck Chemicals	Cat# S7128
C24	Laboratory of Dr. Greg Wang (UNC Chapel Hill)[31]	N/A
UNC7043	Laboratory of Dr. Lindsey James (UNC Chapel Hill)[22]	N/A
UNC6852	Laboratory of Dr. Lindsey James (UNC Chapel Hill)[22]	N/A
MS177	Laboratory of Dr. Greg Wang (UNC Chapel Hill)[31]	N/A

(*Continued on next page*)

Continued

REAGENT or RESOURCE	SOURCE	IDENTIFIER
GST-EZH2-135-200	Laboratory of Dr. Greg Wang (UNC Chapel Hill)[31]	N/A
GST-EZH2-135-200-A/A	Laboratory of Dr. Greg Wang (UNC Chapel Hill)[31]	N/A
GST-EZH2-135-200-A/K	Laboratory of Dr. Greg Wang (UNC Chapel Hill)[31]	N/A
GST-EZH2-135-200-K/A	Laboratory of Dr. Greg Wang (UNC Chapel Hill)[31]	N/A
GST-EZH2-135-200-K/K	Laboratory of Dr. Greg Wang (UNC Chapel Hill)[31]	N/A
Recombinant RelA	Laboratory of Dr. Greg Wang (UNC Chapel Hill)	N/A
Recombinant RelB	Laboratory of Dr. Greg Wang (UNC Chapel Hill)	N/A
Critical commercial assays		
Bradford Protein Assay Reagent	BioRad	Cat# 500-006
Clarity Western ECL Substrate	BioRad	Cat# 1705060
iScript cDNA Synthesis Kit	BioRad	Cat# 1708890
iTaq Universal Probes Supermix	BioRad	Cat# 1725131
Maxima SYBR Green/ROX qPCR Master Mix (2X)	Thermo Fisher Scientific	Cat# K0221
QIAquick PCR Purification Kit	QIAGEN	Cat# 28104
RNeasy Kit	QIAGEN	Cat# 74104
Dual-Glo Luciferase Assay System	Promega	Cat# E2920
QIAprep Spin Miniprep kit	QIAGEN	Cat# 27104
NEBNext Ultra II DNA Library Prep Kit	NEB	Cat# 7103
Deposited data		
Uncropped migration and sphere image data	Mendeley	https://data.mendeley.com/drafts/hggpsm9vnv
ChIP-seq analysis of SUM149 and MDA-MB-231 cells	This manuscript	GSE223959
RNA-seq analysis of SUM149 and MDA-MB-231 cells (siCtrl and siEZH2)	This manuscript	GSE223959
RNA-seq analysis of MDA-MB-231 cells (siCtrl, siRelA, and siRelB)	This manuscript	GSE223959
Experimental models: Cell lines		
HEK293T	ATCC	Cat# CRL-11268; RRID:CVCL_0063
MDA-MB-231	ATCC	Cat# HTB-26; RRID:CVCL_0062
MDA-MB-231 TetOn-shEV	This manuscript	N/A
MDA-MB-231 TetOn-shEZH2	This manuscript	N/A
SUM149	Laboratory of Dr. Charles Perou (UNC Chapel Hill)	RRID:CVCL_3422
Oligonucleotides		
ChIP-qPCR primer oligonucleotides	IDT	See Table S6, related to STAR Methods
qPCR Taqman primer-probe sets	Thermo Fisher Scientific	See Table S6, related to STAR Methods
siCtrl (siGENOME Non-Targeting Control siRNA #5)	Horizon Discovery (Dharmacon)	Cat# D-001210-05

(*Continued on next page*)

Continued

REAGENT or RESOURCE	SOURCE	IDENTIFIER
siEZH2 (siGENOME siRNA – SMARTpool)	Horizon Discovery (Dharmacon)	Cat# M-004218-03
siRelA (siGENOME siRNA – SMARTpool)	Horizon Discovery (Dharmacon)	Cat# M-003533-02
siRelB (siGENOME siRNA – SMARTpool)	Horizon Discovery (Dharmacon)	Cat# M-004767-02
siSUZ12 (siGENOME siRNA – SMARTpool)	Horizon Discovery (Dharmacon)	Cat# M-006957-00
siEED (siGENOME siRNA – SMARTpool)	Horizon Discovery (Dharmacon)	Cat# M-017581-01
Recombinant DNA		
psPAX2	Addgene	Cat# 12260; RRID:Addgene_12260
pMD2.5G	Addgene	Cat# 12259; RRID:Addgene_12259
p1242 3x-KB-L	Laboratory of Dr. Albert Baldwin (UNC Chapel Hill)[79]	Cat #26699; RRID:Addgene_26699
pRP[Pro]-hRluc-{RELB_1.7kb}	This manuscript	VectorBuilder ID VB220112-1274kts
pRL-TK-Renilla	Promega	Cat# E2231
Lenti-pCDH-TetOn-shEV	Laboratory of Dr. Greg Wang (UNC Chapel Hill)[31]	N/A
Lenti-pCDH-TetOn-shEZH2	Laboratory of Dr. Greg Wang (UNC Chapel Hill)[31]	N/A
pCDH-HA-EZH2	Laboratory of Dr. Greg Wang (UNC Chapel Hill)[31]	N/A
pCDH-HA-EZH2-TAD_A	Laboratory of Dr. Greg Wang (UNC Chapel Hill)[31]	N/A
pCDH-HA-EZH2-TAD_K	Laboratory of Dr. Greg Wang (UNC Chapel Hill)[31]	N/A
pcDNA3-FLAG-EV	Laboratory of Dr. Wenyi Wei (Harvard University)	N/A
pcDNA3-FLAG-EZH2	Laboratory of Dr. Wenyi Wei (Harvard University)	N/A
pcDNA3-FLAG-RelA	Laboratory of Dr. Albert Baldwin (UNC Chapel Hill)	N/A
Software and Algorithms		
cutadapt	Martin[96]	https://github.com/marcelm/cutadapt
STAR v2.5.2b	Dobin et al.[97]	https://github.com/alexdobin/STAR
MACS2	Zhang et al.[98]	https://github.com/macs3-project/MACS
HOMER	Heinz et al.[64]	http://homer.ucsd.edu/homer/
salmon	Patro et al.[100]	https://github.com/COMBINE-lab/salmon
DESeq2	Love et al.[101]	https://github.com/mikelove/DESeq2
Hisat v2.0.5	Kim et al.[102]	https://github.com/DaehwanKimLab/hisat2
featureCounts v1.5.0-p3	Liao et al.[103]	https://www.rdocumentation.org/packages/Rsubread/versions/1.22.2/topics/featureCounts
FASTX-Toolkit	Hannon Lab, CSHL	http://hannonlab.cshl.edu/fastx_toolkit/index.html
BEDTools	Quinlan and Hall[99]	https://github.com/arq5x/bedtools2
MSigDB (v2022.1.Hs updated 8/2022); HALLMARK and GOBP gene sets	Subramian et al.; Liberzon et al.; Ashburner et al.; Carbon et al.[104–106,108]	https://www.gsea-msigdb.org/gsea/msigdb/

(*Continued on next page*)

Continued

REAGENT or RESOURCE	SOURCE	IDENTIFIER
PANTHER (Released 221013); GO-Slim BP gene set (v17.0 Released 220222)	Mi et al.; Ashburner et al.; Carbon et al.[105–107]	http://pantherdb.org
MRI Wound Healing Tool plugin for ImageJ	Jonkman et al.[109]	https://github.com/MontpellierRessourcesImagerie/imagej_macros_and_scripts/wiki/Wound-Healing-Tool
cBioPortal (TCGA, METABRIC)	Gao et al., Cerami et al.[84,85]	https://www.cbioportal.org
Other		
Ultra-low attachment 6-well plates	Corning	Cat# 3471
ChIP-seq data (H3K27me3, H3K4me3, input)	Messier et al.[59]	GSE77772
ChIP-seq and ATAC-seq data (ATAC, H3K4me1, H3K27ac, input)	Takaku et al., Tanaka et al.[60,61]	GSE72141

RESOURCE AVAILABILITY

Lead contact

Further information and requests for resources and reagents should be directed to and will be fulfilled by the lead contact, Albert S Baldwin (abaldwin@med.unc.edu).

Materials availability

All plasmids generated in this study are available on request.

Data and code availability

- Raw and processed ChIP-seq and RNA-seq data have been deposited to GEO under accession GSE223959 and are publicly available as of the date of publication. Uncropped microscopy images have been deposited as a Mendeley Dataset. All data reported in this paper will be shared by the lead contact upon request. This paper analyzes existing, publicly available data. All accession numbers and links are listed in the key resources table.
- This paper does not report original code.
- Any additional information required to reanalyze the data reported in this paper is available from the lead contact upon request.

EXPERIMENTAL MODEL AND STUDY PARTICIPANT DETAILS

Cell lines

HEK293T (*Homo sapiens*, female, RRID: CVCL_0063), MDA-MB-231 (*Homo sapiens*, female, RRID: CVCL_0062), and MDA-MB-231-derived stably expressing cell lines (TetOn-shEV and TetOn-shEZH2) were grown in DMEM basal media supplemented with 10% FBS (Gibco) at 37°C and 5% CO_2. SUM149 (*Homo sapiens*, female, RRID: CVCL_3422) cells were grown in HuMEC basal media supplemented with 5% FBS, and HuMEC supplement kit (Gibco) at 37°C and 5% CO_2. Independent STR profiling and mycoplasma contamination screening to authenticate cells was performed by Genetica DNA Laboratories (Burlington, NC) prior to use in experiments.

METHOD DETAILS

Transfection and generation of cell lines

HEK293T, SUM149, or MDA-MB-231 cells were seeded and allowed to adhere in 10cm dishes for passaging. Transfection was performed with Dharmafect I (Dharmacon) for siRNA (20nM, see key resources table) or FuGene HD (Promega) for plasmids (0.75 μg/mL, see key resources table) prepared in OptiMEM (Gibco). Cells were harvested 48 hours after transfection unless otherwise indicated. Lentivirus was prepared using the psPAX2 and pMD2.5G packaging system co-transfected for 48 hours in HEK293T cells. Supernatant containing virus was passed through 0.45μM filters (Pall Corporation), and applied to target

cells with 8ug/mL polybrene (EMD Millipore). Stable cell lines were further selected using 1ug/mL puromycin (Thermo Fisher Scientific) or Geneticin (Gibco) for 7 days before validation.

Reverse transcription quantitative PCR

RNA was isolated from cells using phenol-chloroform (5:1) extraction with TRIzol Reagent (Invitrogen) followed by precipitatation with 2 volumes isopropanol, wash with 4 volumes 70% ethanol, and resuspension in 20uL nuclease-free water (Corning). RT performed with 1ug total RNA using iScript cDNA Synthesis Kit (BioRad) according to manufacturer's instructions. qPCR was performed using iTaq universal primers (BioRad) and TaqMan primer-probe sets (Thermo Fisher Scientific, see Table S6), and quantified using the delta-delta Ct method against housekeeping gene *GUSB*.

Immunoblotting and signal quantification

Cells were harvested in lysis buffer (1% Triton X-100, 150mM NaCl, 20mM Tris pH 8, 1mM EDTA, 1mM EGTA, 0.1% SDS, 1mM beta-glycerol-phosphate, 1mM Na-pyrophosphate) with fresh protease and phosphatase inhibitors on ice for 10 min before pelleting debris for 10 min at 13,000 rpm. Lysate concentration was measured using Bradford assay (BioRad) against a standard of bovine serum albumin (BSA), and samples were prepared with 4X SDS buffer (BioRad) and 10X dithiothreitol (DTT, Thermo Fisher Scientific) and boiled at 95°C for 5min. Equal amounts of protein were separated by SDS-PAGE on 4-15% gradient Mini-Protean-TGX (BioRad), transferred to nitrocellulose membranes (Pall 66485) followed by appropriate overnight primary and 1h secondary antibody incubations (see key resources table). Following Clarity Western enhanced chemiluminescence (ECL) detection (BioRad), blots were imaged using ChemiDoc platform (BioRad). Densitometry was quantified using ImageJ and normalized to beta-Actin or GAPDH loading controls.

Chromatin immunoprecipitation (ChIP) qPCR

ChIP was performed with an adapted disuccinimidyl glutarate (DSG) and formaldehyde chromatin crosslinking protocol (Wang 2022, Tian 2012, Singh 2019). 2-5x10^6 cells were collected in PBS, fixed with 2mM DSG reagent (Thermo Fisher Scientific) for 45min rotating at room temperature, washed, fixed with 1% formaldehyde (Thermo Fisher Scientific) for 10 min rotating at room temperature, and quenched with 125mM glycine rotating for 5 min at room temperature. Fixed cells were lysed in Buffer 1 (50mM HEPES-KOH, 140mM NaCl, 1mM EDTA pH 8, 10% glycerol, 0.5% NP-40, 0.25% Triton X-100, freshly supplemented protease and phosphatase inhibitors) by rotation for 10 min at 4°C, pelleted for 5 min at 3000 rpm at 4°C, lysed in Buffer 2 (10mM Tris-HCl pH8, 200mM NaCl, 1mM EDTA pH8, 0.5mM EGTA, freshly supplemented protease and phosphatase inhibitors) by rotation for 10 min at 4°C, pelleted for 5 min at 3000 rpm at 4°C, and resuspended in Buffer 3 (10mM Tris-HCl pH8, 100mM NaCl, 1mM EDTA pH8, 0.5mM EGTA, 0.1% NaDOC, 0.5% N-laurylsarcosine, freshly supplemented protease and phosphatase inhibitors) for sonication. Cells were sonicated on High for 30min with 30sec on/off in a water bath sonicator maintained at 4°C (Diagenode). 10% Triton X-100 was added to sonicated lysates and spun at 11,000rpm for 10 min at 4°C to pellet debris; 5% input and the appropriate number of aliquots were taken from sonicated lysate. Following overnight antibody incubation and incubation with BSA-blocked Dynabeads (beads washed in RIPA buffer were incubated with 0.1ug/uL BSA for 30min followed by RIPA wash) for 1h at room temperature, beads were sequentially washed in low salt (20mM Tris-HCl pH8, 150mM NaCl, 2mM EDTA pH8, 1% Triton X-100, 0.1% SDS), high salt (20mM Tris-HCl pH8, 500mM NaCl, 2mM EDTA pH8, 1% Triton X-100, 0.1% SDS), and LiCl (250mM LiCl, 10mM Tris-HCl pH8, 1mM EDTA pH8, 1% NP-40, 1% NaDOC) buffers. DNA was eluted with Elution buffer (1% SDS, 100mM NaHCO3) and agitation for 15 min at 42°C. ChIP and input DNA was reverse crosslinked with RNaseA (0.2 mg/mL) and NaCl (20mM) for 2h at 65°C and Proteinase K (0.4 mg/mL) for 1h at 50°C before processing using Qiagen PCR Clean Up Kit per kit protocol. qPCR was performed using Maxima SYBR Green (Thermo Fisher Scientific); percent input of ChIP DNA was calculated from minimum 3-point dilution curve of 5% input DNA in qPCR. Primer sequences can be found in Table S6.

ChIP-seq

ChIP DNA was generated as for qPCR. ChIP-seq libraries (Illumina) were prepared according to manufacturer's recommendations and sequenced at the UNC High Throughput Genomic Sequencing facility using single-end 50bp reads. We then used cutadapt to filter for adaptor contamination and subsequently filtered reads using FASTX-Toolkit such that at least 90% of bases of each read had a quality score

exceeding 20.[96] Duplicated sequences were then capped at a maximum of 5 occurrences, and reads were aligned to the reference human genome (hg19) using STAR version 2.5.2b retaining only primary alignments.[97] Reads aligning to excluded regions as defined by ENCODE were then removed. Reads were then extended in silico to a fragment size of 250 bp, and regions of significant enrichment relative to input control were identified using MACS2.[64,98] Bound genes were defined as any ChIP-seq peak call that overlapped a gene body +/-5kb; bound promoters were defined as any ChIP-seq peak call that overlapped a transcription start site (TSS) +/- 5kb. The longest-annotated isoform was used to obtain unique instances in the case of multiple gene isoforms. Motifs were identified by comparing the 200 bp surrounding the peak midpoint to the 200 bp flanking sequence on either side of each identified peak using HOMER.[64] Histone modification ChIP-seq and ATAC-seq data were obtained from GSE77772 and GSE72141 and were re-processed exactly as described above, except ATAC-seq reads were shifted 5bp to account for the Tn5 insertion, and H3K27me3 peak domains were define dby merging two or more "broad" peaks within 10kb of each other using BEDTools.[99]

RNA-seq

RNA was extracted from SUM149 and MDA-MB-231 cells using RNeasy kit with on-column DNase digestion (QIAGEN). Samples treated with control or EZH2 siRNA (related to Figure 2) were sequenced at the UNC High Throughput Genomic Sequencing facility as single-end 50 bp reads. We then used cutadapt to filter for adapter contamination and subsequently filtered reads using FASTX-Toolkit such that at least 90% of bases of each read had a quality score exceeding 20.[96] Reads were aligned to the reference human genome (hg19) using STAR version 2.5.2b retaining only primary alignments.[97] Reads aligning to excluded regions as defined by ENCODE were then removed. Transcript abundance was then estimated using salmon, and differential expression was detected using DESeq2.[100,101]

Samples treated with control, RelA, or RelB siRNA (related to Figure 3) were sequenced and analyzed by Novogene (Beijing, China) as paired end 150bp reads. Reads were filtered for adaptor contamination and high quality using Novogene in-house perl scripts. Reads were aligned to the reference genome (hg19) using Hisat2 v2.0.5.[102] Transcript abundance was counted using featureCounts v1.5.0-p3 and differential expression detected using DESeq2.[101,103]

Gene set enrichment analysis

Gene Set Enrichment Analysis (GSEA) was performed using either PANTHER Overrepresentation Test tool with Gene Ontology (GO)-Slim Biological Process gene set or the Molecular Signatures Database (MSigDB) tool with HALLMARK and/or Gene Ontology: Biological Process gene sets as indicated in figure legends.[104–108] Results from all tests were considered significant with a False Discovery Rate (PANTHER: Fisher's Exact test; MSigDB: Benjamini and Hochberg correction) of $q<0.05$, and enrichment values are presented as $-\log_{10}(q)$.

Luciferase reporter assay

HEK293T cells seeded in white-walled 96-well plates (Corning) were transfected with: 25ng p1242 3x-KB-L (Baldwin 1991) and 25ng pRL-TK Renilla (Promega), or 50ng pRP-hRluc-RELB_1.7kb dual reporter construct containing 1.7kb of the RELB promoter sequence (Bren 2001, VectorBuilder); for co-transfections with RelA or EZH2, 50ng of pcDNA-FLAG-RelA, pCDH-HA-WT-EZH2 or pCDH-HA-TAD_A-EZH2 or pCDH-HA-TAD_K-EZH2 were used. After 48 hours luminescence was measured using Dual Luciferase Reporter Assay (Promega) according to manufacturer instructions and luciferase signal was normalized to Renilla control. Plasmid details can be found in key resources table.

Immunoprecipitation and HA-IP

Cells were lysed in IP buffer (0.1% NP-40, 50mM Hepes-NaOH ph8, 150mM NaCl) with fresh protease and phosphatase inhibitors on ice for 10 min before pelleting debris for 10 min at 13,000 rpm at 4°C. Lysate concentration was determined using Bradford Assay against BSA standards. 5% input, mock IP, and target antibody IP aliquots were taken from equal concentrations of lysate. For immunoprecipitation, antibody was incubated for 3 hours before addition of Protein G magnetic beads for 1 hour. For HA-IP, HA-conjugated magnetic beads (Thermo Fisher Scientific) were incubated in lysates for 3 hours. Protein G or HA beads were washed 3x in IP buffer, and protein was eluted by boiling in 2X SDS buffer (BioRad) before addition of 10X DTT and separation by SDS-PAGE, transfer to nitrocellulose membranes, and immunoblotting with

appropriate primary (overnight) and secondary (1h) antibodies. CleanBlot detection reagent (Thermo Fisher Scientific) was used in place of secondary antibody for blots of proteins with predicted molecular weight 50-75kDa (RelA and RelB) to avoid interference of immunoglobulin heavy chain signal. Clarity Western ECL reagents and ChemiDoc were used to detect and image blots.

GST fusion recombinant protein pulldown

GST pulldown was conducted with HEK293T cell lysate and 1 μg of GST fusion and other recombinant protein. Cells were lysed in EBC buffer (120mM NaCl, 0.5% NP-40, 5ug/mL leupeptin, 10ug/mL aprotinin; 50ug/mL PMSF, 0.2mM sodium orthovanadate, 100mM NaF, 50mM Tris-Cl pH8) with fresh protease and phosphatase inhibitors on ice for 10 min before pelleting debris for 10 min at 13,000 rpm, and lysate used for GST pulldown.[31]

Migration assay

MDA-MB-231 TetOn-shEV or TetOn-shEZH2 cells were treated with 2ug/mL doxycycline for 48 hours before seeding in 6-well plates, followed by transient transfection with EV or WT or mutant TAD EZH2 expression vectors. After 36 hours, wells were rinsed and cells serum starved 12h in Opti-MEM medium. Wells were then scraped in a 'plus' shape using a 1000uL pipette tip to create a wound, rinsed with PBS to remove debris, replenished with serum-free media, and imaged once per arm of the 'plus' for a total of 4 data points per well ("0h"). Following 24h of migration, wells were imaged again in the same manner and positions ("24h"). Wound closure was measured and quantified using ImageJ plugin MRI Wound Healing Tool according to author instructions.[109]

Tumorsphere assay

For stable cell lines: MDA-MB-231 TetOn shEZH2 cells, or TetOn shEZH2 cells additionally stably expressing WT or mutant TAD EZH2 were treated with or without 2ug/mL doxycycline for 72h on adherent 10cm dishes before detaching and seeding at $2x10^4$ cells/well in ultra-low adherence 6-well plates (Corning) in basal Mammocult media (STEMCELL Technologies). For siRNA or PROTAC treatment: MDA-MB-231 cells were treated with respective compounds (20nM siRNA; 6.25μM UNC7043/UNC6852; 2.5uM MS177) for 48h on adherent 10cm dishes before detaching and seeding at $2x10^4$ cells/well in ultra-low adherence 6-well plates in basal Mammocult media. After 24h, 96h, and 168h, spheres were imaged ("D1", "D4", "D7"). On D7, spheres were collected, counted, and approximate number calculated as per STEMCELL Technologies protocol for counting spheres.

Soft agar colony formation assay

$24x10^3$ cells/mL were seeded in DMEM supplemented with 0.4% agarose onto 1% agarose-coated wells. 0.5mL of fresh media with compound was added every four days for 3-4 weeks. At the endpoint, cell culture plates were stained overnight with 100ug/mL iodonitrotetrazolium chloride (Sigma) before counting.

QUANTIFICATION AND STATISTICAL ANALYSIS

Graphpad Prism (v9) was used for statistical analysis. For comparisons between two sets of data with assumed normal distribution, unpaired two-tailed Student's t-test was performed. $p<0.05$ was considered statistically significant, and p values are denoted as: *$p<0.05$, **$p<0.01$, ***$p<0.001$, and ****$p<0.0001$. Data are presented as the mean +/- standard distribution from three biologically independent experiments. All data from representative experiments, such as images and blots, and sequencing experiments were repeated at least two independent times.